

# NOTE TO USERS

This reproduction is the best copy available.

**UMI**<sup>®</sup>



University of Alberta

The Structure and Stability of Alkanethiol Self-Assembled  
Monolayers on Gold

by

Jingmin Han



A thesis submitted to the Faculty of Graduate Studies and Research in  
partial fulfillment of the requirements for the degree of Master of Science.

Department of Mechanical Engineering

Edmonton, Alberta

Fall 2004



Library and  
Archives Canada

Bibliothèque et  
Archives Canada

Published Heritage  
Branch

Direction du  
Patrimoine de l'édition

395 Wellington Street  
Ottawa ON K1A 0N4  
Canada

395, rue Wellington  
Ottawa ON K1A 0N4  
Canada

*Your file* *Votre référence*

*ISBN: 0-612-95761-6*

*Our file* *Notre référence*

*ISBN: 0-612-95761-6*

The author has granted a non-exclusive license allowing the Library and Archives Canada to reproduce, loan, distribute or sell copies of this thesis in microform, paper or electronic formats.

L'auteur a accordé une licence non exclusive permettant à la Bibliothèque et Archives Canada de reproduire, prêter, distribuer ou vendre des copies de cette thèse sous la forme de microfiche/film, de reproduction sur papier ou sur format électronique.

The author retains ownership of the copyright in this thesis. Neither the thesis nor substantial extracts from it may be printed or otherwise reproduced without the author's permission.

L'auteur conserve la propriété du droit d'auteur qui protège cette thèse. Ni la thèse ni des extraits substantiels de celle-ci ne doivent être imprimés ou autrement reproduits sans son autorisation.

---

In compliance with the Canadian Privacy Act some supporting forms may have been removed from this thesis.

Conformément à la loi canadienne sur la protection de la vie privée, quelques formulaires secondaires ont été enlevés de cette thèse.

While these forms may be included in the document page count, their removal does not represent any loss of content from the thesis.

Bien que ces formulaires aient inclus dans la pagination, il n'y aura aucun contenu manquant.

# Canada

## ACKNOWLEDGEMENTS

First of all, I wish to express my sincere appreciation to my advisor, Professor Daniel Y. Kwok, for his continual support and helpful suggestion in my research. I sincerely appreciate his patient guidance during the past two years.

I would like to acknowledge my co-advisor, Professor Xiaodong Wang, for his encouragement and counsel.

I also thank Dr. Anthony Yeung to be my examining committee member.

I am grateful to all my colleagues in the Nanoscale Technology and Engineering Laboratory (NTEL), especially Kelvin Isaacson. I sincerely appreciate their help over the past two years.

I would like to thank my mother and my sister for helping me become who I am today.

I also regret being unable to be with my son, Jiang Renze, during the past two years, and I cannot wait to be with him soon. I also thank my parents-in-law for taking care of my son during my study.

Finally, I would like to express my deepest gratitude for the understanding and love that I received from my best friend and husband, Jiang Bo. With his thoughtful advice and continued encouragement, I have finally completed my graduate study.

# CONTENTS

<b>1</b>	<b>Introduction</b>	<b>1</b>
<b>2</b>	<b>Literature Review</b>	<b>5</b>
2.1	SAMs' Structure . . . . .	5
2.1.1	The Structure of Alkanethiol . . . . .	5
2.1.2	SAMs' Formation Process . . . . .	5
2.1.3	The Structure of SAMs on Au(111) . . . . .	9
2.2	SAM's Stability . . . . .	15
2.2.1	Mechanical Stability . . . . .	15
2.2.2	Thermal Stability . . . . .	16
<b>3</b>	<b>Substrate Preparation</b>	<b>19</b>
3.1	Materials . . . . .	19
3.2	Substrate Evaporation . . . . .	20
3.3	Substrate Pretreatment . . . . .	20
<b>4</b>	<b>SAMs' Structure</b>	<b>25</b>
4.1	Experimental Section . . . . .	25

4.2	Structure of SAMs on Au/Cr/Si Substrate . . . . .	27
4.3	Structure of SAMs on Au/Ti/Si Substrate . . . . .	30
4.4	Thickness Measurements . . . . .	33
<b>5</b>	<b>SAMs' Stability</b>	<b>35</b>
5.1	Experiment Setup . . . . .	35
5.2	Mechanical Stability of SAMs on Au/Cr/Si substrate . . . . .	37
5.2.1	SAMs on evaporated Au/Cr/Si surface . . . . .	39
5.2.2	SAMs on chemically etched Au/Cr/Si . . . . .	39
5.3	Mechanical Stability of SAMs on Au/Ti/Si substrate . . . . .	43
5.3.1	SAMs on evaporated Au/Ti/Si surface . . . . .	43
5.3.2	SAMs on chemically-etched Au/Ti/Si surface . . . . .	46
5.3.3	SAMs on annealed Au/Ti/Si . . . . .	46
5.4	Ellipsometric Measurements . . . . .	51
<b>6</b>	<b>Discussion</b>	<b>53</b>
6.1	SAMs on Au/Cr/Ti substrates . . . . .	53
6.2	SAMs on Au/Ti/Si substrates . . . . .	55
6.3	Simulation . . . . .	56
<b>7</b>	<b>Conclusions</b>	<b>59</b>
7.1	Conclusions . . . . .	59
7.2	Future Work . . . . .	60
	<b>Bibliography</b>	<b>62</b>

## LIST OF TABLES

2.1	Thermal stability of thiol-based SAMs on Au in hot solvents. Half-lives were estimated <i>ex situ</i> by changes in ellipsometric thickness (T: Temperature) . . . . .	17
2.2	Advancing $\theta_a$ and receding $\theta_r$ contact angles (deg.) of water on $\text{CH}_3(\text{CH}_2)_{11}\text{SH}$ adsorbed onto Au(111) for various annealing procedures. Modified from [1] E. Delamarche, B. Michel, H. Kang and C. Gerber, <i>Langmuir</i> , 10, 4103 (1994) . . . . .	18
4.1	Description of Vibrational Modes of C-H Stretching for Polycrystalline Alkyl-S Chains[2, 3]. (Abbreviations used: $\nu$ = vibration mode, asym = asymmetric, sym= symmetric, ip=in plane, op=out of plane, FR=Fermi resonance splitting component,    = parallel, $\perp$ = perpendicular) . . . . .	29



## LIST OF FIGURES

1.1	Schematic illustration of a self-assembled organic monolayer adsorbed on a metal surface. The surface properties can be varied by changing the end functional group. . . . .	2
2.1	Schematic of self-assembled monolayer layout. Angle $\alpha$ refers to tilt of molecular axis with respect to substrate surface normal. Twist angle, $\psi$ , describes rotation about axis of molecule.	6
2.2	Schematic mechanistic diagram for the self-assembly of SAM on Au(111) . . . . .	8
2.3	Schematic of SAMs' structure on Au(111). Basic structure (dashed line parallelogram): $(\sqrt{3} \times \sqrt{3})R30^\circ$ ; superlattice (solid line rectangular): $c(4 \times 2)$ or $(2\sqrt{3} \times 3)$ in units of $a_{Au}$ , as indicated in the figure . . . . .	10
2.4	A schematic view of odd and even cases for a tilted alkanethiol on Au. The odd alkyl chain length positions the terminal C-C bond more parallel to the plane of the surface when compared to the even alkyl chain length. . . . .	13

3.1	Schematic illustration of a typical evaporation system used for the preparation of Au substrates . . . . .	21
3.2	AFM images of evaporated Au (a) and annealed Au (b) for a scan size of 1 $\mu\text{m}$ . . . . .	24
4.1	FTIR spectra of SAMs formed on Au/Cr/Si surface by different pretreatment methods. (a) on evaporated surface; (b) on piranha-etched surface; (c) on annealed surface . . . . .	28
4.2	FTIR spectra of SAMs formed on Au/Ti/Si surface by different pretreatment methods. (a) on evaporated surface; (b) on piranha-etched surface; (c) on annealed surface . . . . .	31
4.3	Schematic illustration of SAM assembly on two different Au substrates. The upper figure demonstrates SAM assembly of $\text{CH}_3(\text{CH}_2)_{17}\text{SH}$ adsorbed onto non-annealed Au with smaller Au steps. The lower figure illustrates SAM assembly of $\text{CH}_3(\text{CH}_2)_{17}\text{SH}$ adsorbed onto annealed Au with larger terraces. . . . .	34
5.1	Schematic experimental setup for SAMs' mechanical stability measurement by an aquasonic cleaner . . . . .	36
5.2	Schematic figure on the cavitation and implosion during ultrasonic cleaning . . . . .	38
5.3	FTIR spectra of SAMs formed on freshly evaporated Au/Cr/Si substrates (a) before sonication; (b) after sonicating for 7 hours	40

5.4	FTIR spectra of SAMs formed on piranha-etched Au/Cr/Si surface subjected to ultrasonic vibration at various duration . . . . .	41
5.5	Schematic illustration of an alkanethiolate adsorbed onto piranha-etched Au/Cr/Si surface before and after sonication. The arrows indicate the transition dipole moments for the following stretching modes: $\nu_a(\text{CH}_3)$ , $\nu_s(\text{CH}_3)$ , $\nu_a(\text{CH}_2)$ , $\nu_s(\text{CH}_2)$ . The intensities of the infrared bands for these transition dipole moments depend on their projection along the surface normal. . . . .	44
5.6	FTIR spectra of SAMs formed on evaporated Au/Ti/Si surface (a) before sonication; (b) after sonicating for 7 hours. . . . .	45
5.7	FTIR spectra of SAMs formed on chemically etched Au/Ti/Si surface (a) before sonication, (b) after sonicating for 7 hours . . . . .	47
5.8	FTIR spectra of SAMs formed on annealed Au/Ti/Si surface subjected to ultrasonic vibration at various duration. . . . .	48
5.9	Schematic illustration of an alkanethiolate adsorbed onto annealed Au/Ti/Si surface before (a) and after (b) sonication. The arrows indicate the transition dipole moments for the following stretching modes: $\nu_a(\text{CH}_3)$ , $\nu_s(\text{CH}_3)$ , $\nu_a(\text{CH}_2)$ , $\nu_s(\text{CH}_2)$ . The intensities of the infrared bands for these transition dipole moments depend on their projection along the surface normal. . . . .	50
5.10	SAMs' thickness variation under sonication . . . . .	51

## NOMENCLATURE

Au .....	Gold
Cr .....	Chromium
Ti .....	Titanium
Si .....	Silicon
S .....	Sulfur
SAM .....	Self-Assembled Monolayer
AFM .....	Atomic Force Microscopy
FTIR .....	Fourier Transform Infra-Red
STM .....	Scanning Tunneling Microscopy
$\text{CH}_3(\text{CH}_2)_{17}\text{SH}$ .....	Octadecanethiol
$\nu_s(\text{CH}_3)$ .....	Symmetric Methyl Bond
$\nu_a(\text{CH}_3)$ .....	Anti-symmetric Methyl Bond
$\nu_s(\text{CH}_2)$ .....	Symmetric Methylene Bond
$\nu_a(\text{CH}_2)$ .....	Anti-symmetric Methylene Bond

# CHAPTER 1

## INTRODUCTION

A recent advance in the fabrication of nanoscale coatings is the use of the so-called Self-Assembled Monolayers (SAMs) [4–7]. SAMs are two-dimensional organic assemblies that form by the spontaneous adsorption of molecules onto metal or metal oxide supports. Alkanethiols, carbon chains with a sulfur atom at one end, are the most popular material to produce SAMs. They form stable, flat monolayers on gold (Au) via a Au-S bond at one end, and can have different surface properties via modification of functional groups at the other end. The organic and biological properties of these films are largely controlled by the end groups of the molecules and can be manipulated by tailoring the end functional groups. A schematic of SAMs is shown in Figure 1.1. SAMs are of technical interest for the fabrication of sensors, protective layers and patternable materials [8]. They provide a pathway for a better understanding of many technological systems where interfacial events play a dominant role. The history of SAMs can be traced to the earlier papers of Zisman et al. [9], where glass surfaces were exposed to dilute solutions of long-

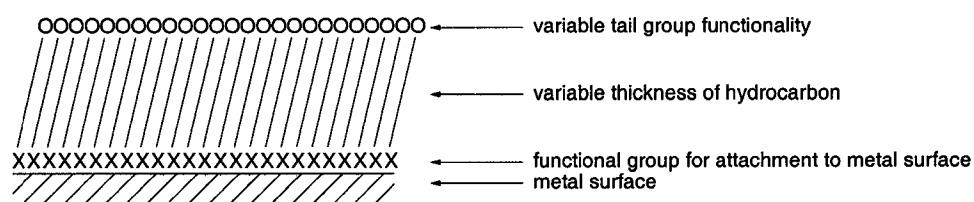


Figure 1.1: Schematic illustration of a self-assembled organic monolayer adsorbed on a metal surface. The surface properties can be varied by changing the end functional group.

chained alcohols in hexadecane. Oriented monolayer films were then formed on the substrate that were not wetted by the solvent. Zisman et al. further studied various surfactant-like molecules including long-chained amines, carboxylic acids and amides on metal and metal oxide surfaces [10, 11]. The systems considered by Zisman et al. exhibit only modest stabilities and were limited only to low-energy hydrophobic surfaces. Nuzzo et al. [12] later extended Zisman's approach by relying on a stronger and more specific interactions between S and Au for molecular self-assembly. The specific interaction between Au and S allows adsorption of thiols not only onto Au, but also other surfaces such as silver, copper, mercury, GaAs and InP. The mechanism of such self-assembly originated from a large reduction of interfacial driving energy for the metal substrates. This specific adsorption is stronger than the physisorbed molecular films by the Langmuir-Blodgett technique which relies on physical packing of molecules and subsequently transfer to surfaces. Self-assembled monolayers (SAMs) derived from the adsorption of organothiols onto Au have been extensively investigated for studying their

potential uses as corrosion inhibitors, resist layers, components of chemical sensors, and models for organic and biological surfaces. Because of the level of adhesion between the deposited Au film and the Si substrate is weak, an adhesion promotion layer has always been used to enhance Au adhesion on Si substrates. The ductile nature of Ti and Cr, together with the fact that both materials are carbide forming elements, makes them promising candidates for use as interlayer materials. In the literature, SAMs are always formed on Au/Cr/Si [12–18] or Au/Ti/Si [19–21] substrates. However, Cr diffuses more easily to the Au surface, weakening the interactions between S and Au. Thus, SAMs' stability on Au/Cr/Si and Au/Ti/Si can be very different.

As organic molecules from the environment are easily adsorbed onto the high energy Au surfaces, complete wetting on Au cannot be achieved under ambient conditions. The properties of Au surfaces have been the subject of considerable work [22–24]; and the importance of the cleanliness of Au surface has been recognized. Typically, one of the following surface pretreatment is used [21, 23, 25–27]: (1) evaporated Au (no treatment); (2) chemical etching; (3) oxygen plasma; (4) sonication. The quality of SAMs' formation depends on the pretreatment method. On an evaporated Au surface, SAMs are relatively less densely-packed due to the contaminants previously adsorbed on the substrate. However, all the previously mentioned pretreatment processes result in a relatively rough surface. Specifically, chemical etching leaves an oxide on the Au surface, reducing SAMs' stability on Au. In this thesis, a

flame annealing pretreatment method was used to clean the Au surface which also reduces the surface roughness. SAMs formed on annealed Au/Ti/Si surface are more crystalline and densely-packed than on those evaporated and piranha-etched Au substrate.

The properties of *n*-alkanethiolate SAMs on Au have been extensively studied in recent years. They are largely motivated by the numerous potential applications of these easily prepared monolayers. Among these applications, stability becomes a limiting factor. For alkanethiol molecules formed on Au, its stability depends on the strength of the Au-S bond and the van der Waals force among thiol molecules. Stable SAMs can only be obtained by alkanethiol molecules self-assembly on smooth and clean Au. Moreover, SAMs' structure and stability also depend on their surface preparation procedures. In the literature, no one has systematically studied the relationship between surface preparation, SAMs' structure and stability. As sonication is typically one of the many cleaning procedures, we study SAMs' stability under sonication conditions. During sonication, an upward periodic tensile load is applied to SAMs because of cavitation [28]. This is an excellent way to characterize the mechanical stability of SAMs. Results from this study will also benefit other interdisciplinary research in Micro Electro Mechanical Systems (MEMS) and ultrasonic microfluidics [29].

This thesis documents the structure and stability of alkanethiol SAMs formed on various Au substrates and reports the relation between surface preparation, SAMs' structure and stability.



## CHAPTER 2

### LITERATURE REVIEW OF SAMs' STRUCTURE AND STABILITY

#### 2.1 SAMs' Structure

##### 2.1.1 The Structure of Alkanethiol

The most popular SAMs' system is that of *n*-alkanethiol ( $\text{HS}(\text{CH}_2)_{n-1}\text{CH}_3$ ) formed on Au(111). The structure of the molecular backbone is schematically showed in Figure 2.1. A tilt angle with respect to the surface normal  $\alpha$  and the angle of molecular twisting about the axis  $\psi$  are typically used to describe the structure of the molecular backbone formed on Au. In principle, the molecular backbone is fully extended if the gauche-defects in the alkane chains are not considered [30].

##### 2.1.2 SAMs' Formation Process

Self-assembled monolayers (SAMs) are formed spontaneously by immersion of metal substrate into organic molecular solution with concentrations in the micromolar to millimolar range [30]. The Au(111) surface is the lowest energy surfaces, which is thus preferred for the growth of thin films [6, 30].

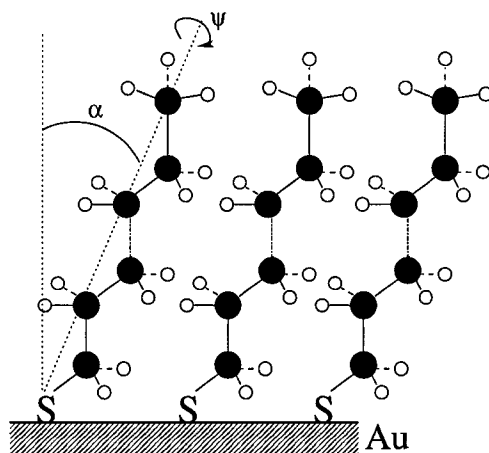


Figure 2.1: Schematic of self-assembled monolayer layout. Angle  $\alpha$  refers to tilt of molecular axis with respect to substrate surface normal. Twist angle,  $\psi$ , describes rotation about axis of molecule.

Thus, alkyl molecular chains that self assemble on Au(111) substrate is considered to be a model system [30]. The kinetics and mechanism for the solution-phase adsorption of *n*-alkanethiols onto Au have been monitored in the literature using *ex situ* Quartz Crystal Microbalance (QCM), Scanning Tunneling Microscope (STM) [25] and an Atomic Force Microscopy (AFM) by Doudevski et al. [31]. The adsorption process of octadecanethiol onto Au has been confirmed to consist of two steps: A fast but disordered adsorption as a first step and a thermodynamically controlled rearrangement as the final step for uniform packing of octadecanethiol [32]. During the first step, the octadecanethiol molecules immediately physisorb onto Au with the molecular axis of their hydrocarbon chains oriented parallel to the surface. As the surface coverage increases to near saturation, a two-dimensional phase transition occurs and produces islands composed of molecules with their hydrocarbon axes oriented at  $\sim 30^\circ$  from the surface normal. Continued exposure to the thiol solution results in a greater number of these islands and growth of these nuclei until SAM is formed with a commensurate structure. A schematic for SAMs' formation process is shown in Figure 2.2.

It is also known that the adsorption rate of octadecanethiol onto Au surfaces increases as the solution concentration of octadecanethiol solution increases. In a 0.1 mM octadecanethiol solution, it takes approximately 800 seconds for the monolayer to completely form over the surface; while only 560 and 120 seconds required for a 1 mM solution and 10 mM solution in hexane respectively [25]. Nevertheless, Karpovich and Blanchard observed

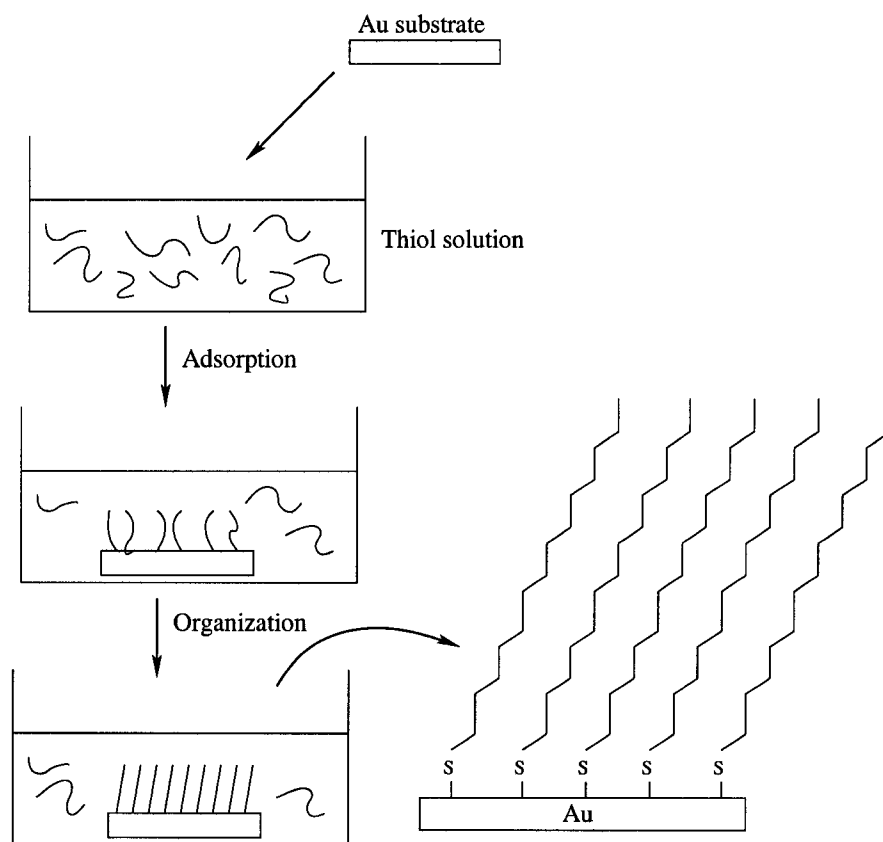


Figure 2.2: Schematic mechanistic diagram for the self-assembly of SAM on Au(111)

a monotonous increase of an initial growth rate with concentration and reported that the adsorption rate of octadecanethiol becomes independent of concentration for a much higher concentration [33].

### 2.1.3 The Structure of SAMs on Au(111)

#### 2.1.3.1 Basic Structure

For alkanethiols formed on Au(111), the S atom seats onto the fcc site, directly above a 3-fold hollow site without a Au atom in the second layer beneath the S atom. This is the lowest energy adsorption site of thiol on Au(111) [34–36]. With the Au at their bulk value, the unit of nearest-neighbor spacing of substrate,  $a_{Au}$ , is 2.88 Å. Thus, these hollow sites are 4.99 Å apart. The final equilibrium full-coverage phase structure of SAMs on Au is when the molecules form a commensurate, triangular ( $\sqrt{3} \times \sqrt{3}$ )R30° overlayer on Au(111). The distance between the thiol atoms is  $\sqrt{3} \times a_{Au}$ . The molecules tilted at 30° with respect to the surface normal (Figure 2.3) [37–40]. This structure corresponds to an area per molecule of 21.6 Å<sup>2</sup>. For the projection onto the 2D plane, one expects an area of 18.4 Å<sup>2</sup> for a straight hydrocarbon chain [41]. Assuming that molecules remain densely packed, this difference would suggest that the axis of the hydrocarbon chains is tilted away from the normal by about  $\alpha = \sim \arccos(18.4/21.6) = \sim 32^\circ$ , consistent with earlier FTIR studies [19, 39]. The basic structure of SAMs on Au is shown in the dashed line parallelogram in Figure 2.3.

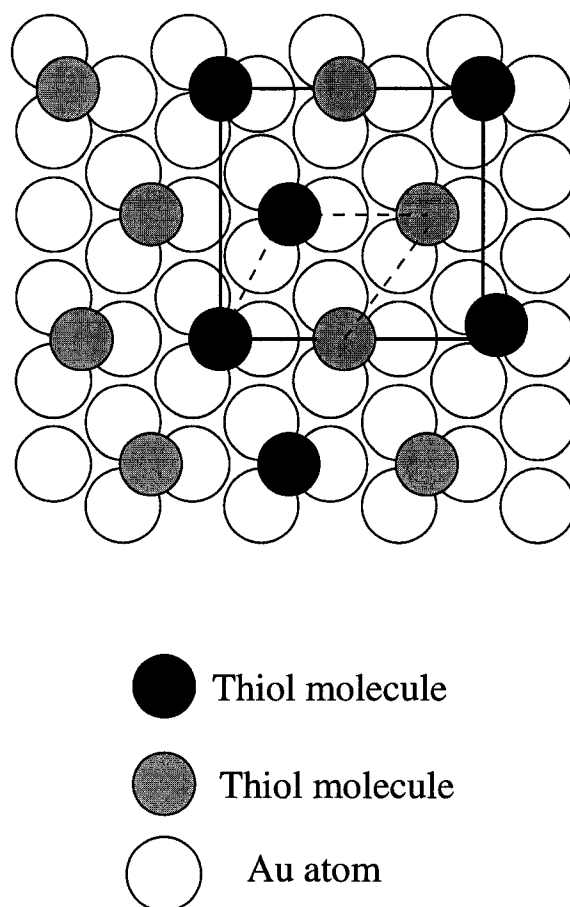


Figure 2.3: Schematic of SAMs' structure on Au(111). Basic structure (dashed line parallelogram):  $(\sqrt{3} \times \sqrt{3})R30^\circ$ ; superlattice (solid line rectangular):  $c(4 \times 2)$  or  $(2\sqrt{3} \times 3)$  in units of  $a_{Au}$ , as indicated in the figure

### 2.1.3.2 Superlattice

All experiments performed to date suggest that monolayers consist of more than one kind of orientations of the chain backbones. The structures of pure alkyl thiol SAMs are more complex than the above  $(\sqrt{3} \times \sqrt{3})R30^\circ$  basic structure. A breakthrough concerning the structure of the above SAMs system was reported in 1994 by Camillone and co-workers [42]. Using He-diffraction, they found that the structure of carefully annealed alkyl thiol SAMs contains four chains per unit cell and is a commensurate  $c(4 \times 2)$  overlayer (Figure 2.3). This finding has now been independently confirmed by the grazing-incidence X-ray diffraction studies by Fenter et al. [43, 44] and the STM experiments of Poirier et al. [45]. From the diffraction experiments, Fenter and coworkers were also able to shed light on the structure of the alkyl thiol SAMs near the Au surface. They reported that high quality diffraction data can only be fitted by assuming the formation of disulfide bridges [44]. In addition, the STM measurements clearly show that the surface of these monolayers exhibit a repeating pattern of bright and dark spots that correspond to a  $c(4 \times 2)$  superlattice of a basic  $(\sqrt{3} \times \sqrt{3})R30^\circ$  overlayer with four thiolate molecules in each unit cell. The experimental results [42–48] lead to suggestion of a model with two (inequivalent) chains per unit cell (c.f. Figure 2.3). The solid line rectangular  $(2\sqrt{3} \times 3)$  pattern in units of nearest-neighbor spacing of Au,  $a_{Au}$ , stands for the superlattice  $c(4 \times 2)$  based on a hexagonal coordinate system; the solid circles stand for the thiol molecules with different twisting angles.

### 2.1.3.3 Odd and Even Effect

Hybridization is the mixing of “atomic orbitals” (i.e., s-, p-, d-) to form new atomic orbitals. By quantum calculations, Sellers et al. [36] found that there are two chemisorption modes for thiolates on Au(111). In the first modes, the surface-S-C bond angle is  $\approx 180^\circ$  (sp hybridization); while the second is  $\approx 104^\circ$  ( $sp^3$  hybridization). The process of hybridization in which one s-orbital and three p-orbitals overlap to produce four hybrid-orbital is known as  $sp^3$ -hybridization. For sp hybridization, the bonds are directly along a linear chain. In the case of saturated *n*-alkanethiol onto Au(111), the trend in the odd-even effect observed in FTIR [2, 49, 50] (reflecting different orientations of the terminal methyl group) clearly implies a preference of  $sp^3$  hybridization in the sulfur atom (or a bended Au-S-C bond angle) and a trans-zig-zag extension of the alkyl chain [51]. Angelico et al. [20] measured SAMs’ structure of *n*-alkanethiol  $CH_3(CH_2)_nSH$  ( $n = 14-17$ ) on Au by FTIR, and confirmed the  $sp^3$ -hybridization Au-S-C bond and a trans-zig-zag extension of the alkyl chain. The higher asymmetric methyl mode  $\nu_a(CH_3)$  and lower symmetric methyl mode  $\nu_s(CH_3)$  absorption arises for the odd number of chains than the even number [52]. The odd-even dependence of the methyl orientation at the chain terminus confirms an all trans conformational arrangement for the alkyl chains. A schematic illustration of odd and even alkanethiol on Au is shown in Figure 2.4.



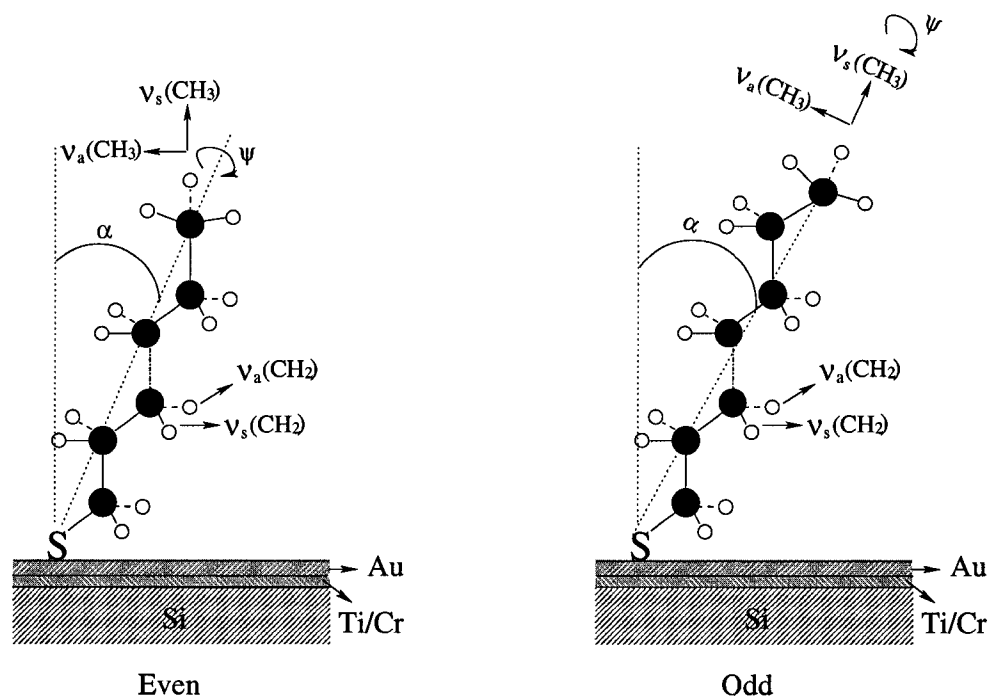


Figure 2.4: A schematic view of odd and even cases for a tilted alkanethiol on Au. The odd alkyl chain length positions the terminal C-C bond more parallel to the plane of the surface when compared to the even alkyl chain length.

#### 2.1.3.4 Chain Length Effect

As indicated in Figure 2.1, the molecules assemble in a slightly tilted, all-trans configuration in order to optimize the lateral interactions between molecules within the monolayer. Different degrees of crystallinity (all-trans in nature) are obtained, depending on the alkylic chain length [53]. The longer the chain, the more the all trans configuration becomes thermodynamically favourable. As a rule of thumb, alkanethiols with chains shorter than 10-12 methylene units form rapidly increasing fractions of gauche conformers, located at the outermost portion of the alkyl chain. Porter et al. [54] were the first to study the effect of chain length on the properties of monolayers in a series of *n*-alkanethiols  $\text{CH}_3(\text{CH}_2)_n\text{SH}$  ( $n = 1, 3, 5, 7, 9, 11, 15, 17, 21$ ). The structure of the above monolayers were characterized by optical ellipsometry, FTIR and electrochemistry. These techniques show that there are distinct differences in structure between long- and short-chain thiol monolayers. The FTIR spectroscopic and ellipsometric data indicate that long-chain thiols form a densely-packed, crystalline-like assembly with fully extended alkyl chains tilted from the surface normal by  $20 - 30^\circ$ . As the chain length decreases, the structure becomes increasingly disordered with less packing density and surface coverage; as the total attractive energy of chain-chain interactions decreases, the coverage and both the intra- and interchain order decrease. As a result, shorter chain length thiol molecules on Au are more likely to be thermally desorbed [38]. Therefore,  $\text{CH}_3(\text{CH}_2)_{17}$  SAM on Au is always used to stand for typical SAMs's structure.

## 2.2 SAM's Stability

Various factors and conditions can degrade the quality of SAMs. The following sections summarize results from the literature where SAMs have purposely been destroyed or tested for their limits of stability by exposure to various conditions. These data provide limits on the useful operating ranges and lifetimes of these SAMs across a variety of conditions.

### 2.2.1 Mechanical Stability

The mechanical stability of thiol-based SAMs on Au was examined by Crooks and coworkers [55, 56] using an interfacial-force microscope (IFM) and a sharpened tungsten tip (tip radius  $\approx 500$  nm and contact area diameter  $\approx 10$  nm). It was found that, in the force profile for the *n*-hexadecanethiol  $\text{CH}_3(\text{CH}_2)_{15}\text{SH}$  SAM, there exist three distinct regions. First, prior to tip contact, there was no evidence of appreciable attractive forces. This is consistent with the expected low surface energy for the methyl-terminated SAM surface. Second, after contact with the SAM surface, the force profile initially shows a rather soft repulsive interaction up to a force of  $\sim 0.8 \mu\text{N}$  which became considerably stiffer as the compression proceeded. Third, upon withdrawal, the interfacial force drops to zero at distances smaller than the initial contact separation with no evidence of an attractive interaction. These compressive loading-cycle data are reducible to within the noise level, for cycle periods of several seconds. From the results [56], they also found no adhesive tip-substrate interaction between *n*-docosanethiol  $\text{CH}_3(\text{CH}_2)_{21}\text{SH}$  SAM on

Au and the tip. Their results indicate that *n*-alkanethiolate SAMs can spontaneously rearrange themselves in the lowest-energy state upon film compression. In addition, SAMs under compressive load show a load-rate-dependent hysteresis in the compressive strain recovery, indicating that the mechanical properties of the SAM are best described by an anelastic model [55–58]. It is the monolayer film’s anelastic property that allows us to measure the structural changes of SAMs under compressive force. The mechanical response of SAMs under tension is still poorly understood because very few techniques can provide the *in situ* investigation of the behavior. One of the objectives in this thesis is to study SAMs’ behavior under a tensile force due to sonication.

### 2.2.2 Thermal Stability

The thermal stability of SAMs has been investigated extensively. In general, thiol-based SAMs desorb quickly from surfaces when placed in a hot solvent than in thermal annealing [1, 13, 17, 59–61]. Bain et al. [13] had examined the effect of chain length on thermal desorption of five methyl-terminated thiols ( $C_{10}$ ,  $C_{12}$ ,  $C_{16}$ ,  $C_{18}$ , and  $C_{22}$ ) in hexadecane at 83°C. Upon heating, the monolayers desorbed and the extent of desorption was monitored by changes in ellipsometric thickness. Table 2.1 summarizes the rates of *ex situ* desorption for various thiol-based SAMs on Au.

Various studies have examined the thermal stability of SAMs in air or vacuum [1, 59, 60, 62]. Delamarche et al. [1] examined the stability of dodecanethiol SAMs on Au(111). Their XPS results of samples annealed at 115°C for

Table 2.1: Thermal stability of thiol-based SAMs on Au in hot solvents. Half-lives were estimated *ex situ* by changes in ellipsometric thickness (T: Temperature)

compound	metal	solvent <sup>†</sup>	T (°C)	1/2 life (min.)	ref.
CH <sub>3</sub> (CH <sub>2</sub> ) <sub>9</sub> SH	Au	HD	83	< 5	[13]
CH <sub>3</sub> (CH <sub>2</sub> ) <sub>11</sub> SH	Au	HD	83	~ 5	[13]
CH <sub>3</sub> (CH <sub>2</sub> ) <sub>15</sub> SH	Au	HD	83	~ 18	[13]
CH <sub>3</sub> (CH <sub>2</sub> ) <sub>17</sub> SH	Au	HD	83	~ 70	[13]
CH <sub>3</sub> (CH <sub>2</sub> ) <sub>21</sub> SH	Au	HD	83	~ 180	[13]
	Au	DHN	84	~ 160	[17]
	Au	DHN	103	~ 10	[17]

<sup>†</sup> HD: hexadecane; DHN: decahydronaphthalene

10 h suggested the formation of alkylsulfonates. For annealing times of 40 h, the carbon signal suggested a loss of material. The produced sulfonates are unstable on Au and removed easily by rinsing with most solvents [63]. The change in surface coverage of SAMs was also evident by wetting. The advancing contact angles of water decreased from 108 ° to 92 ° upon heating for 10 h at temperatures of 85 to 130 °C, while the receding angles decreased from 100 to 66 ° [1]. The wetting results suggest surface energy changes due to structural rearrangement and/or desorption of the thiols from the surface [Table 2.2]. STM experiments suggested that an annealing temperature of 100 °C constitutes a reasonable trade off between SAM's reorganization and disruption [1, 59]. The ultra-high vacuum (UHV) desorption of alkanethiolate SAMs on Au has been the subject of several recent studies [64–68].

Table 2.2: Advancing  $\theta_a$  and receding  $\theta_r$  contact angles (deg.) of water on  $\text{CH}_3(\text{CH}_2)_{11}\text{SH}$  adsorbed onto Au(111) for various annealing procedures. Modified from [1] E. Delamarche, B. Michel, H. Kang and C. Gerber, Langmuir, 10, 4103 (1994)

sample	$\theta_a$	$\theta_r$	$\theta_a - \theta_r$
annealed for 10 h at			
85°C	108	100	8
100°C	109	99	10
115°C	104	88	16
130°C	92	66	26
annealed at 100 °C for			
2 h	107	96	11
10 h	109	99	10
18 h	105	94	11
40 h	104	92	12

## CHAPTER 3

### SAMS' SUBSTRATE PREPARATION

This chapter details the procedures for SAMs' substrate preparation. Au is thermally evaporated onto Si wafer, with either Cr or Ti as an interlayer to enhance the adhesion. As organic contaminants are easily adsorbed on high energy Au surface, chemical etching and flame annealing are usually used to clean the Au substrate before SAMs' adsorption.

#### 3.1 Materials

Si wafers of test grade were obtained from Wafer World (West Palm Beach, FL) in circular disks of about 10 cm diameter and were cut into rectangular shapes of about 2.5 cm  $\times$  5 cm. Au shot (99.999%), Cr shot (99.995%) and Ti shot (99.995%) were obtained from Kurt J. Lesker (Clairton, PA). Ethanol (100%) was obtained from the Chemistry Department at the University of Alberta.  $\text{CH}_3(\text{CH}_2)_{17}\text{SH}$  (98%) was obtained from Aldrich Chemical Company and used as received. Piranha solution was made just before used ( $\text{H}_2\text{SO}_4$  :  $\text{H}_2\text{O}_2 = 3 : 1$ , *Caution: Piranha reacts violently with organic material!*)

### 3.2 Substrate Evaporation

The most commonly employed method for preparing Au thin film has been the evaporation of Au onto a flat Si wafer. Since the level of adhesion between the deposited Au film and these supports is weak, an interlayer of chromium or titanium of  $\sim 10$  nm is often used to enhance the adhesion. A schematic illustration of the evaporation system is shown in Figure 3.1. A requirement for adhesion by these materials is that vacuum must be maintained between the evaporations of the adhesion layer and the Au. Au/Cr/Si substrates for this experiment were prepared by sequentially evaporating  $\sim 100$  Å Cr and  $\sim 1000$  Å Au onto small rectangular Si wafers in a diffusion-pumped vacuum chamber at a rate of  $\leq 2$  Å/s under  $2 \times 10^{-6}$  Torr. Au/Ti/Si substrates were prepared by sequentially evaporating  $\sim 100$  Å Ti and  $\sim 1000$  Å Au onto small pieces of Si wafers under the same condition. Au prepared by evaporation at room temperature is typically polycrystalline and has a predominately (111) structure. Au(111) has a close-packed, 3-fold symmetric structure. Once Au(111) substrate is immersed into thiol solutions, the thiol atoms would adsorb directly on a 3-fold hollow site. This is the lowest energy adsorption site of thiol onto Au(111) [34–36].

### 3.3 Substrate Pretreatment

Organic contaminants are easily adsorbed onto high energy Au surfaces. Thus, complete wetting on these surfaces cannot be obtained in laboratory ambient. The contaminants can be removed by chemical etching or flame an-



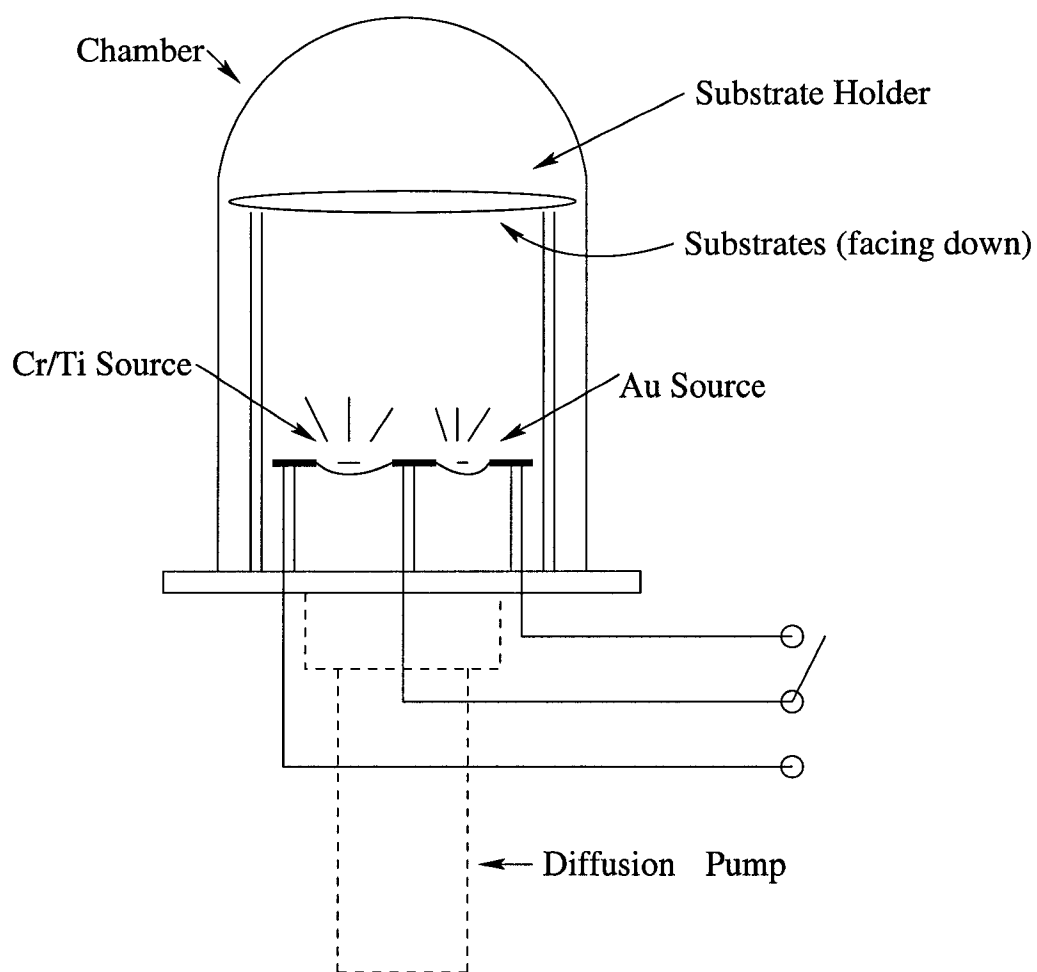
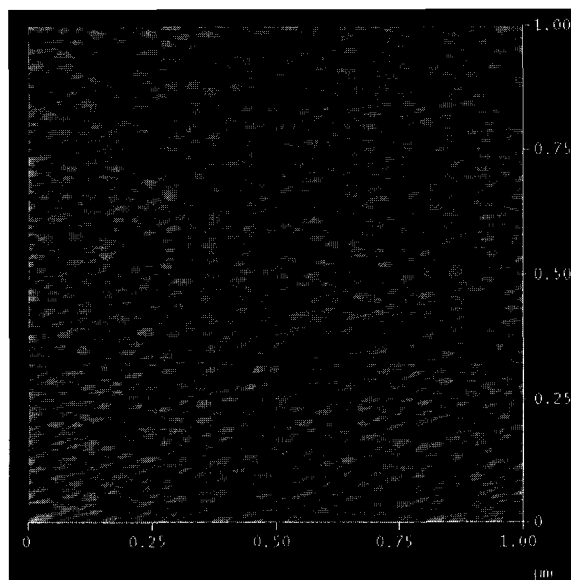


Figure 3.1: Schematic illustration of a typical evaporation system used for the preparation of Au substrates

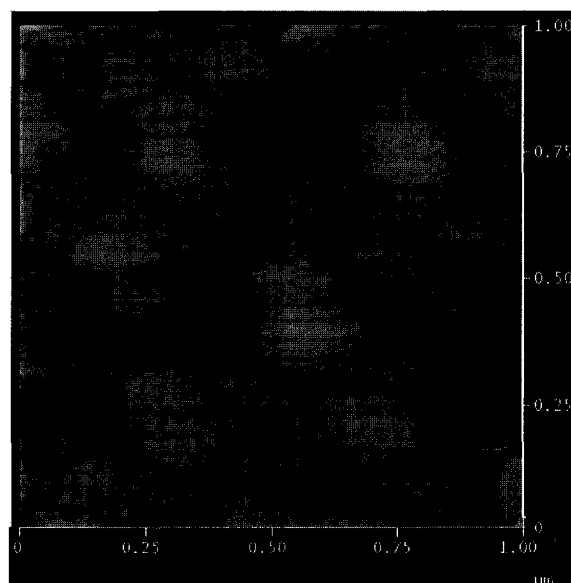
nealing. To compare the effects of various pretreatments on SAMs' structure and stability, we restricted our study on both the Au/Cr/Si and Au/Ti/Si substrates for three types of pretreatment procedures: (1) freshly evaporated surfaces (just left in the as-deposited condition); (2) piranha-etched surfaces; and (3) annealed surfaces. One group of Au/Cr/Si substrates were immersed into piranha solution ( $\text{H}_2\text{SO}_4 : \text{H}_2\text{O}_2 = 3 : 1$ , *Caution: Piranha reacts violently with organic material!*) for 5 minutes, and then rinsed with ethanol; Another group of Au/Cr/Si substrates were flame annealed over a Bunsen burner for  $\sim 45$  seconds at  $\sim 1$  Hz frequency; the remaining Au/Cr/Si substrates just left untreated (i.e. freshly evaporated). The Au/Ti/Si substrates were prepared by the same evaporation and pretreatment procedures as the Au/Cr/Si substrates. All experiments were conducted in laboratory ambient.

The piranha-etched and flame-annealed Au surfaces were not only identified by the lack of surface contaminations, but also by the difference in surface structure. Creager et al. [26] conducted Scanning Tunneling Microscopy (STM) measurement to compare the difference between the evaporated and chemically etched Au surfaces. When the Au surface was chemically etched, part of the Au was removed. Thus, after chemical etching, the Au surface appears to be macroscopically rough. Although the etched surface exhibited ridge-like and fairly large macroscopic features, it was microscopically much smoother than the surface of the evaporated Au surface; hence, SAMs formation is anticipated to have fewer defects [26]. In contrast, the evaporated

Au surface is made up of smaller domains ( $\sim 50$  nm) and has a “rolling hills” topology. The surface consists of crystallites of  $40$  nm  $\times$   $80$  nm and typical peak-to-valley heights of  $3$  nm between grains [26, 69, 70]. This feature reflects the nucleation-growth mechanism of film formation when Au condenses from the vapor phase onto a substrate at room temperature. Annealing the Au substrate removes most organic contaminants and shaves the “rolling hills” on the evaporated Au surface. The high temperature during annealing leads to Au surface restructuring [71], and causes the fusion of small domains into larger ones ( $\sim 200$  nm). This result was confirmed by our Atomic Force Microscopy results (Figure 3.2). The Atomic Force Microscopy (AFM) measurements were performed using a Digital Instruments Nanoscope IIIa atomic force microscope (Digital Instruments, Santa Barbara, CA). Standard Si nitride cantilevered probes were used with a force/spring constant in the range between  $0.06 - 0.58$  N/m. The AFM images of annealed and evaporated Au surfaces were captured by using contact mode. The surfaces were cut into  $1$  cm  $\times$   $1$  cm samples to fit onto a  $1.5$  cm  $\times$   $1.5$  cm sample stage. AFM images shown in Figure 3.2 suggest that the annealed Au has larger terraces (as much as  $200$  nm); while that of the evaporated Au has much smaller steps ( $\sim 50$  nm).



(a)



(b)

Figure 3.2: AFM images of evaporated Au (a) and annealed Au (b) for a scan size of  $1 \mu\text{m}$

## CHAPTER 4

### SAMs' STRUCTURE

This chapter details SAMs' structure on evaporated, piranha-etched and annealed Au/Cr/Si and Au/Ti/Si substrates. SAMs' structure vary dramatically, depending on different substrate pretreatment methods.

#### 4.1 Experimental Section

**SAMs' Formation** SAMs were prepared by immersing all substrates into 1 mM of  $\text{CH}_3(\text{CH}_2)_{17}\text{SH}$  in ethanol overnight. The  $\text{CH}_3(\text{CH}_2)_{17}\text{SH}$  molecules self-assemble on the substrates and form a typical SAM structure onto Au surface [54]. The resulting surfaces were rinsed with ethanol and blown dry by nitrogen before use. All experiments were conducted in laboratory condition.

**Spectroscopic Ellipsometry** SAMs were first characterized by a Sopra GESP5 Variable Angle Spectroscopic Ellipsometer. The ellipsometry measurements were performed using a rotating polarizer in the tracking analyzer mode. A broad band of light (300 to 850 nm) from a 75 W Xe-arc lamp is linearly polarized and directed onto the film surface at an incident angle of

75° from the surface normal. The  $\tan \Psi$  and  $\cos \Delta$  for each bare Au substrate were measured as references immediately after evaporation. After immersion into 1 mM of octadecanethiol/ethanol solution overnight, a new set of  $\tan \Psi$  and  $\cos \Delta$  for each substrate were measured again using an ambient-film-substrate model for regression with known refractive index ( $n$  and  $k$ ) for  $\text{CH}_3(\text{CH}_2)_{17}\text{SH}$  adsorbed onto Au. The refractive index for  $\text{CH}_3(\text{CH}_2)_{17}\text{SH}$  adsorbed onto Au as a function of wavelength was independently obtained from a Sopra GXR Grazing X-ray Reflectometer, rather than assuming an index of refraction (e.g.  $n = 1.46$ ) at a given wavelength (e.g.  $\lambda = 6328 \text{ \AA}$ ) as typically performed in the literature. Such spectroscopic measurements are expected to provide more accurate results in ellipsometer thickness since the optical constants for a range of wavelengths were used simultaneously. The thickness was calculated according to the following equation

$$(\tan \Psi)e^{(i\Delta)} = f(n_i, k_i, T_i) \quad (4.1)$$

where  $n$  and  $k$  are the optical constants of the film and  $T$  is its thickness; subscript  $i$  represents different wavelength. Ellipsometric measurements were conducted at three locations on each sample, and averaged for its thickness. At least five samples were used for each pretreatment process. The averages of thickness for each situation were used to represent the thickness of SAMs on the Au/Cr/Si and Au/Ti/Si substrates under various time of sonication.

**Infrared Measurements** Fourier Transform Infrared (FTIR) spectra of SAM of  $\text{CH}_3(\text{CH}_2)_{17}\text{SH}$  onto Au were obtained using a ThermoNicolet Nexus 670 spectrometer equipped with a VeeMax grazing angle accessory. A p-polarized light was incident at  $75^\circ$  from the surface normal and the reflected light was detected by means of a MCT-A detector cooled with liquid nitrogen. The spectra resolution was  $2\text{ cm}^{-1}$ . Spectra were referenced to the corresponding bare Au substrates (freshly evaporated, piranha-etched and annealed) and 1024 scans were obtained for better signal-to-noise ratios. An infrared gain of 2 was selected for all FTIR measurements to ensure that the input FTIR signals are constant. Samples were rinsed with ethanol and blown dry by  $\text{N}_2$  prior to characterization. The data presented have not been manipulated except for baseline correction.

#### 4.2 Structure of SAMs on Au/Cr/Si Substrate

It is well-known that the peak positions of the symmetric as well as the antisymmetric  $\text{CH}_2$  stretching vibrations can be used as a sensitive indicator of the ordering of the alkyl chains [16]. Figure 4.1 displays FTIR spectra for SAMs derived from  $\text{CH}_3(\text{CH}_2)_{17}\text{SH}$  on freshly evaporated, piranha-etched and annealed Au/Cr/Si substrates (the surface preparation procedures have been discussed in Chapter 3). Table 4.1 shows the C-H stretching frequency for crystalline SAMs on Au. For all-trans zig-zag, highly-ordered conformations, the  $\nu_a(\text{CH}_2)$  and  $\nu_s(\text{CH}_2)$  modes are typically observed below  $2850$  and  $2920\text{ cm}^{-1}$ , respectively. In Figure 4.1, the  $\nu_a(\text{CH}_2)$  and  $\nu_s(\text{CH}_2)$  peak

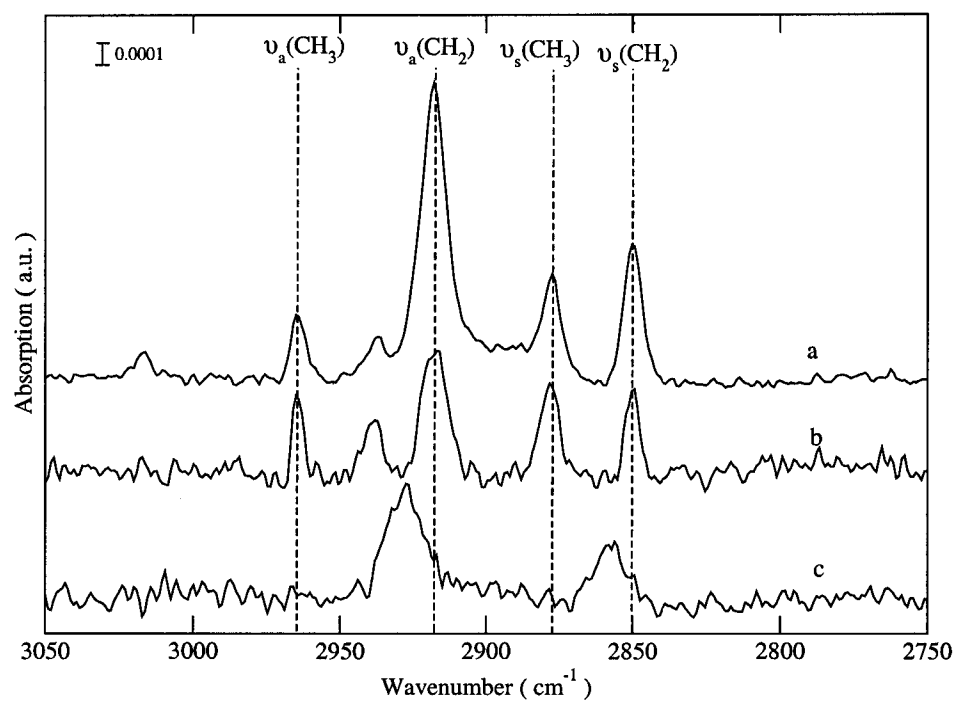


Figure 4.1: FTIR spectra of SAMs formed on Au/Cr/Si surface by different pretreatment methods. (a) on evaporated surface; (b) on piranha-etched surface; (c) on annealed surface



Table 4.1: Description of Vibrational Modes of C-H Stretching for Polycrystalline Alkyl-S Chains[2, 3]. (Abbreviations used:  $\nu$  = vibration mode, asym = asymmetric, sym = symmetric, ip=in plane, op=out of plane, FR=Fermi resonance splitting component,  $\parallel$  = parallel,  $\perp$  = perpendicular)

mode description	peak frequency( $\text{cm}^{-1}$ )	assigned direction of transition dipole moment
$\nu_a(\text{CH}_3)(\text{ip})(r_a^-)$	2964	ip CCC backbone, $\perp$ C-CH <sub>3</sub> bond
$\nu_a(\text{CH}_3)(\text{op})(r_b^-)$	2957	$\perp$ CCC backbone
$\nu_s(\text{CH}_3\text{-FR})(r^+)$	2935	$\parallel$ C-CH <sub>3</sub> bond
$\nu_a(\text{CH}_2)(d^-)$	2918	$\perp$ CCC backbone plane
$\nu_s(\text{CH}_3)(r^+)$	2879	$\parallel$ C-CH <sub>3</sub> bond
$\nu_s(\text{CH}_2)(d^+)$	2850	ip CCC backbone plane

positions for the SAMs formed on evaporated Au/Cr/Si and piranha-etched Au/Cr/Si surfaces are exactly at 2918 and 2850  $\text{cm}^{-1}$ , respectively. According to above guideline, SAMs formed on evaporated and piranha-etched Au/Cr/Si substrates have highly crystalline structures while SAMs on annealed Au/Cr/Si substrate are in a liquid-like state (Figure 4.1). SAMs formed on evaporated Au surface have pronounced intensities of the  $\nu_a(\text{CH}_2)$  and  $\nu_s(\text{CH}_2)$ . This feature indicates that SAMs are less densely-packed and have a relatively larger tilt angle from the surface normal [6, 16]. The organic contaminants on the evaporated Au surface can be removed by chemical etching or annealing. Compared to SAMs on freshly evaporated Au, the intensity of  $\nu_a(\text{CH}_2)$  and  $\nu_s(\text{CH}_2)$  of SAMs formed on piranha-etched Au were smaller than on evaporated Au. These results suggest that SAMs formed on piranha-etched Au surface are more densely-packed with a relatively small tilt angle. Thus, there was not much methylene exposed to the SAMs' sur-

face [16]. Scanning Tunneling Microscopy (STM) measurement conducted by Creager et al. suggested that chemically etched surfaces exhibit fairly large macroscopic features, but microscopically much smoother than the surface of the evaporated Au, resulting in fewer SAMs' defects.

Although annealing Au/Cr/Si substrates also removed the organic contaminants, crystalline SAMs' structure cannot be obtained as Cr easily diffuses to the Au film during annealing which reduces the Au-S affinity. Figure 4.1c shows the structure of SAMs formed on annealed Au/Cr/Si surface. Not only the peak positions of  $\nu_a(\text{CH}_2)$  and  $\nu_s(\text{CH}_2)$  increase, but also there is no methyl group peak can be observed, suggesting that the thiol molecules are in a liquid-like state on the substrate. Following the annealing procedures as described in the experimental section, no peaks in the FTIR spectra can be observed. While it is true that crystalline SAMs on annealed Au/Cr/Si substrates can also be obtained by increasing the Au thickness to 2000 Å and reducing the annealing time to 15 seconds (before Cr diffuses to Au surface), significant trial and error is required.

### 4.3 Structure of SAMs on Au/Ti/Si Substrate

Following the same pretreatment procedures as Au/Cr/Si substrate, we conducted experiment for SAMs formed on freshly evaporated, piranha-etched and annealed Au/Ti/Si substrates. Figure 4.2 displays FTIR spectra for SAMs derived from  $\text{CH}_3(\text{CH}_2)_{17}\text{SH}$  on the above substrates. The SAMs formed on all these three surfaces appear to be crystalline. However, their

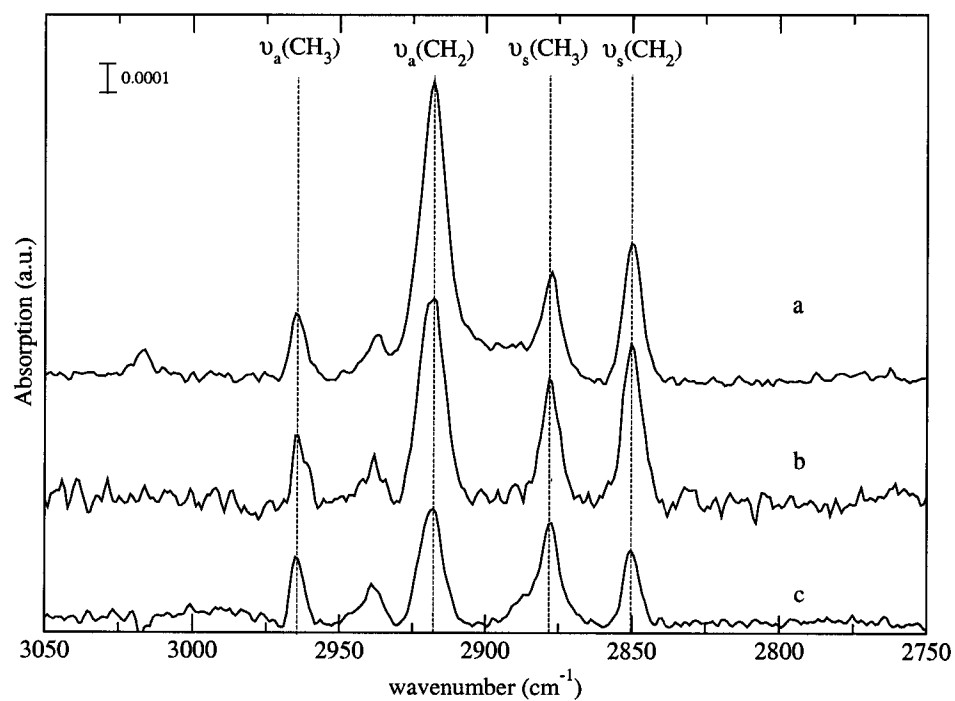


Figure 4.2: FTIR spectra of SAMs formed on Au/Ti/Si surface by different pretreatment methods. (a) on evaporated surface; (b) on piranha-etched surface; (c) on annealed surface

methylene intensities vary dramatically. The intensities of the methylene peaks are largest for the SAMs on freshly evaporated Au, least intense for SAMs on annealed Au, and intermediate on the piranha-etched Au. The differences in  $\nu_a$  ( $\text{CH}_2$ ) intensity reflect different tilt angles for the polymethylene chains on these surfaces. These results suggest that the tilt angle of SAMs on evaporated Au is larger than those on piranha-etched Au, which has a tilt angle larger than that on annealed Au. The tilt of the hydrocarbon chain in SAMs is a result of the packing arrangement for the adsorbates on the metal surface. The higher  $\nu_a$  ( $\text{CH}_2$ ) intensity reflects larger canted orientation and less densely-packed structure [6, 16]. Thus, SAMs formed on evaporated Au/Ti/Si substrate is not densely-packed. This is because organic contaminants in the ambient are adsorbed onto the hydrophilic Au surface. Piranha can remove organic contaminants from the Au surface and result in microscopically smooth domain surface. SAMs formed on piranha-etched surface are more densely packed than those on the evaporated substrates. After evaporation, the Au surface is made up of many small domains ( $\sim 50$  nm), and the surface is relatively rough. Annealing the Au substrate removes most organic contaminants and shaves the "rolling hills" on evaporated Au surface. Ti diffuses through Au more slowly than Cr, and hence annealing the Au/Ti/Si substrate could produce a clean and smooth Au surface. The high temperature during annealing leads to well-known reconstruction [71], and causes the fusion of small domains into larger ones ( $\sim 200$  nm). This result is confirmed by the Atomic Force Microscopy images in Figure 3.2.

SAMs formed on annealed surfaces are more densely-packed, with only a few methylene groups exposed on a well-ordered methyl surface. From the interpretation of the above FTIR and AFM results, we constructed a model in Figure 4.3 that illustrates a possible arrangement of  $\text{CH}_3(\text{CH}_2)_{17}\text{SH}$  adsorbed onto evaporated and annealed Au. From the schematic, it is expected that FTIR would detect more methylenes per unit projected area on the evaporated Au than that for the annealed Au. This is due to the polycrystalline nature of evaporated Au that causes variation of the methyl and methylene groups exposed to surface. The schematic also supports the FTIR results for the lower asymmetric methyl intensity and higher symmetric methyl intensity for SAM on the annealed-Au, as the methyl groups are oriented more toward the surface normal than those on the evaporated one.

#### 4.4 Thickness Measurements

The theoretical thickness of  $\text{CH}_3(\text{CH}_2)_{17}\text{SH}$  monolayer on Au(111) surface, comprising of fully extended alkyl chains tilted  $30^\circ$  from the surface normal, is 22 Å [23]. Ellipsometric measurements were conducted at three locations on each sample, and at least five samples were used for each substrate pretreatment. The average of the measurements confirmed that the thickness of  $\text{CH}_3(\text{CH}_2)_{17}\text{SH}$  monolayer on freshly evaporated, piranha-etched and annealed Au/Ti/Si surfaces is 20, 21 and 22 Å, respectively. These results also agree with FTIR findings shown in Figure 4.2. SAMs formed on annealed Au surfaces are most densely-packed, and its thickness is higher than

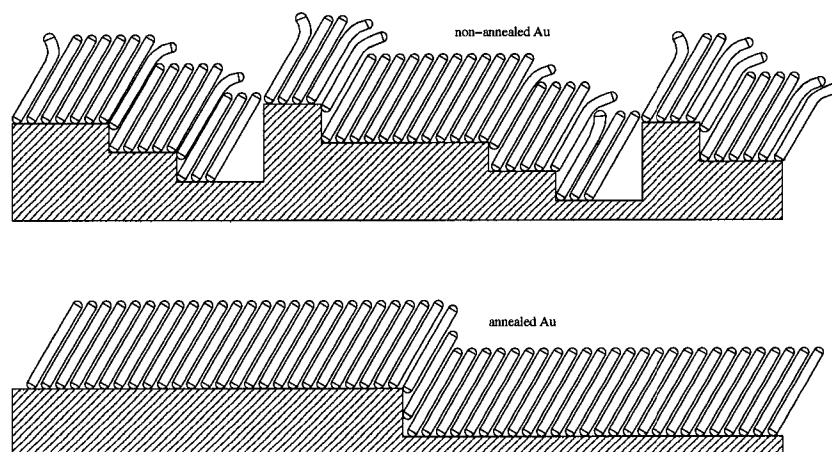


Figure 4.3: Schematic illustration of SAM assembly on two different Au substrates. The upper figure demonstrates SAM assembly of  $\text{CH}_3(\text{CH}_2)_{17}\text{SH}$  adsorbed onto non-annealed Au with smaller Au steps. The lower figure illustrates SAM assembly of  $\text{CH}_3(\text{CH}_2)_{17}\text{SH}$  adsorbed onto annealed Au with larger terraces.

SAMs on piranha-etched and evaporated surfaces. For  $\text{CH}_3(\text{CH}_2)_{17}\text{SH}$  monolayer self-assembled onto evaporated and piranha-etched Au/Cr/Si surface, the thickness is similar to that on the Au/Ti/Si substrate. The exact SAM thickness on annealed Au/Cr/Si surface could not be obtained as Cr diffused extensively to the Au surface in accordance with the FTIR results (Figure 4.2).

## CHAPTER 5

### SAMs' MECHANICAL STABILITY

SAMs formed on evaporated, piranha-etched and annealed Au/Cr/Si or Au/Ti/Si substrates have different structures, and result in different stability. The mechanical stability of the above SAMs were investigated via ultrasonic vibration in ethanol.

#### 5.1 Experiment Setup

For this experiment, an aquasonic cleaner (75D VWR Scientific Product) was used to sonicate the sample surface, which was placed in a 600 ml beaker with 100 ml of ethanol. The beaker was suspended in water inside the sonicator to permit free access of sound waves to the samples. This process is schematically illustrated in Figure 5.1.

During sonication, periodic load is exerted on the SAMs surface by the vibration of ethanol. When ultrasonic energy is introduced, alternating patterns of low and high pressure phases are generated [28]. Liquid is compressed during the high-pressure phase of the wave cycle and pulled apart during the low-pressure phase. Cavities will then grow from microscopic nuclei to a

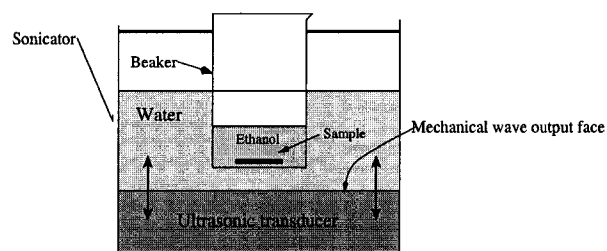


Figure 5.1: Schematic experimental setup for SAMs' mechanical stability measurement by an aquasonic cleaner



maximum critical diameter. During the subsequent high-pressure phase, the cavities are compressed and implode violently. This leads to violent impact waves, whose pressure amplitude exceeds several hundred times that of the ultrasonic oscillation which causes the cavitation. This process results in a strong influence upon the material surface layer. A schematic that describes this process is shown in Figure 5.2.

The samples are immersed into ethanol in the sonicator where the SAMs on the substrates are subjected to an upward periodic load because of cavitation. The force amplitude relates directly to the cavitation intensity, liquid medium, sonication frequency and power. It is noted that liquid medium is an important factor. An ideal medium should have a low surface tension to allow formation of cavitation at low oscillation amplitudes, and good wettability to ensure good contact with the sample [72]. Thus, ethanol was selected as the medium to sonicate the SAMs sample during this experiment. Cavitation intensity is directly related to the ultrasonic power, but is inversely related to the ultrasonic frequency. As the ultrasonic frequency increases, cavitation intensity will reduce because of smaller cavitation bubbles causing less violent implosion. The sonicator has a frequency of 38.5 kHz where its power was set to 90 W for SAMs' stability measurements.

## 5.2 Mechanical Stability of SAMs on Au/Cr/Si substrate

The mechanical response of Au substrates passivated by SAMs has been studied by a number of groups [55, 56]. SAMs under compressive load show

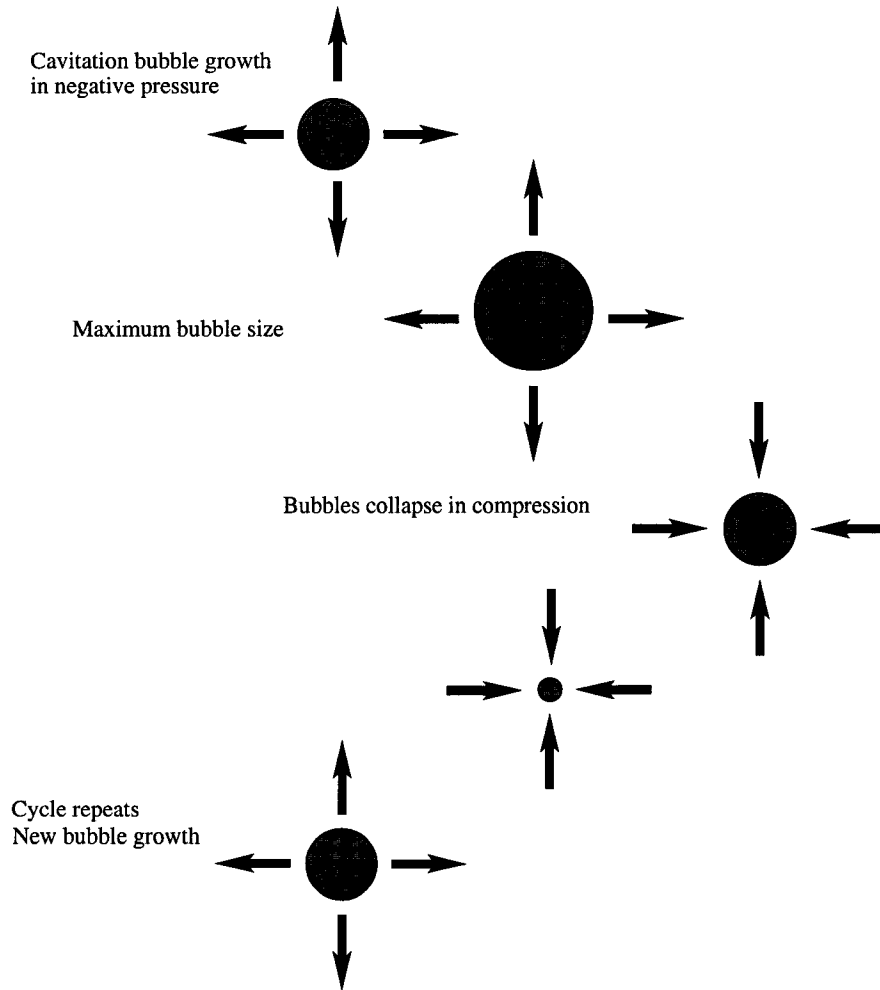


Figure 5.2: Schematic figure on the cavitation and implosion during ultrasonic cleaning

a load-rate-dependent hysteresis in the compressive strain recovery, indicating that the mechanical properties of the SAMs are best described by an anelastic model [55–58]. It is the monolayer film's anelastic property that allows us to *ex situ* measure their structural change. The mechanical response of SAMs under tension is still poorly known because very few techniques can investigate such a behavior. Sonicating the SAMs sample provides an excellent approach to measure its resistance of removal from the substrate.

### 5.2.1 SAMs on evaporated Au/Cr/Si surface

Under sonication, the structure of SAMs formed on evaporated Au surface changes gradually. Figure 5.3 compares the FTIR spectra before and after sonication for SAMs on evaporated Au/Cr/Si surface. After sonicating for 7 hours, the  $\nu_a(\text{CH}_2)$  intensity increases, and its peak band broadens. This indicates that some molecules have been peeled off by the cavitation force, causing the tilt angle to increase, and more methylene group to expose.

### 5.2.2 SAMs on chemically etched Au/Cr/Si

Under sonication, the structure of SAMs on piranha-etched Au surface changes dramatically (Figure 5.4).

1. After sonication, the peak position of  $\nu_a(\text{CH}_2)$  shifts from  $2918\text{ cm}^{-1}$  to a higher wavenumber ( $\sim 2926\text{ cm}^{-1}$ ), and  $\nu_s(\text{CH}_2)$  shifts from  $2849$  to  $2854\text{ cm}^{-1}$ . From our previous discussion in Chapter 4, the higher wavenumber of methylene stretching mode, the more gauche defects

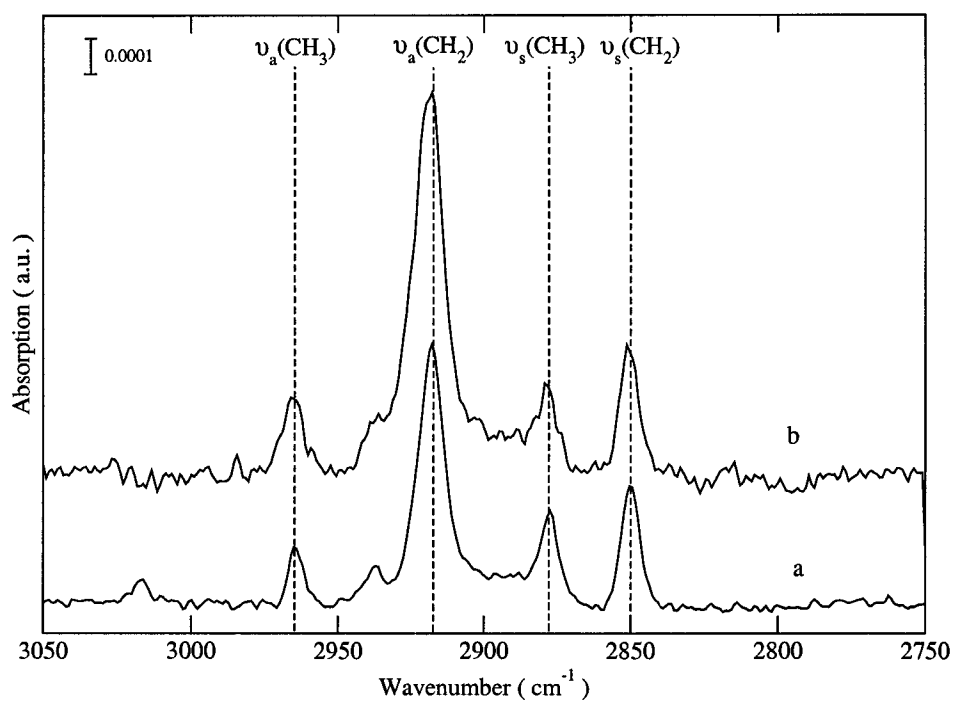


Figure 5.3: FTIR spectra of SAMs formed on freshly evaporated Au/Cr/Si substrates (a) before sonication; (b) after sonicating for 7 hours

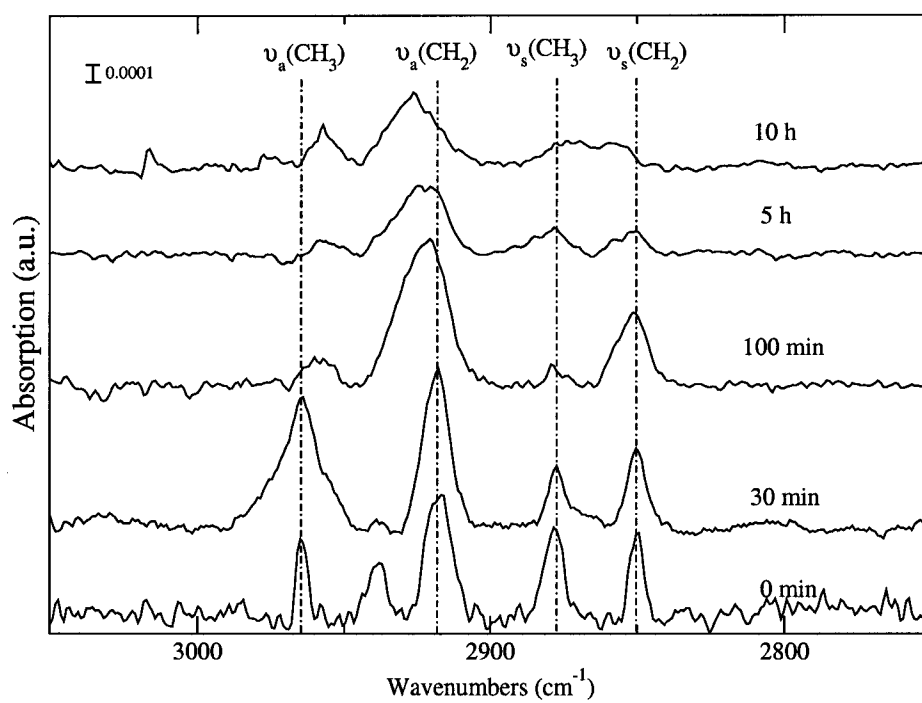


Figure 5.4: FTIR spectra of SAMs formed on piranha-etched Au/Cr/Si surface subjected to ultrasonic vibration at various duration

inside the monolayer on Au.

2. The peak of  $\nu_s(\text{CH}_2)$  and  $\nu_a(\text{CH}_2)$  broaden as the sonication time increases. The  $\nu_a(\text{CH}_2)$  shows a pronounced increase in broadness, partially masking the Fermi resonance component of the  $\text{CH}_3$  stretching mode at  $2938\text{ cm}^{-1}$ . This is another indication about the crystallinity of SAMs. The broadness of these peaks indicates a higher density of gauche defects and less crystalline [16, 32].
3. As the sonication time increases, the peak of  $\nu_a(\text{CH}_3)$  changes from  $2963\text{ cm}^{-1}$  (in CCC backbone plane) to  $2957\text{ cm}^{-1}$  (out of CCC backbone plane), and both  $\nu_a(\text{CH}_3)$  and  $\nu_s(\text{CH}_3)$  intensities decrease. The changes in intensity of  $\text{CH}_3$  are indicative of a larger tilt of the chain axis away from the surface normal, resulting in a decrease in the overall adsorbate density on the surface. The  $\nu_a(\text{CH}_3)$  stretching vibration mode changing from in plane to out of plane indicates that SAMs have become less crystalline with poor coverage on Au surface [73].
4. After sonication for 10 hours, the  $\nu_s(\text{CH}_3)$  peak at  $2878\text{ cm}^{-1}$  is completely lost and only a small  $\nu_a(\text{CH}_2)$  band remains. These results suggest the loss of a significant fraction of the methyl-terminated SAMs, not just orientation change [74].

The changes in the FTIR spectra indicate that SAMs formed on piranha-etched Au/Cr/Si surface are not stable. Possible reasons for its less stability are as follows:

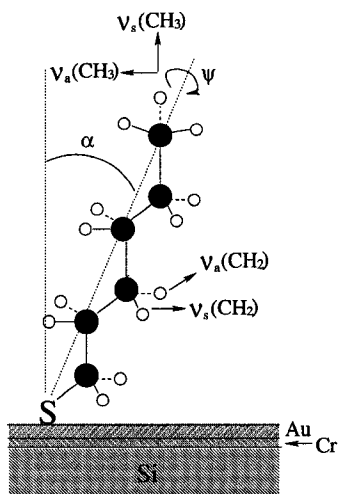
1. Piranha leaves a surface oxide which can affect the properties of SAMs deleteriously [22, 23].
2. When Au film is deeply etched by piranha, the Cr interlayer easily diffuses to the Au surface. Consequently, the bond strength between molecule and substrate is reduced.
3. Piranha-etched Au surface is microscopically smooth and thiol molecules are densely-packed in a small domain; however, the surface is macroscopically rough, resulting in the weak van der Waals forces among molecules.

A schematic model for SAMs' structure on chemically etched Au/Cr/Si substrates before and after sonication are shown in Figure 5.5.

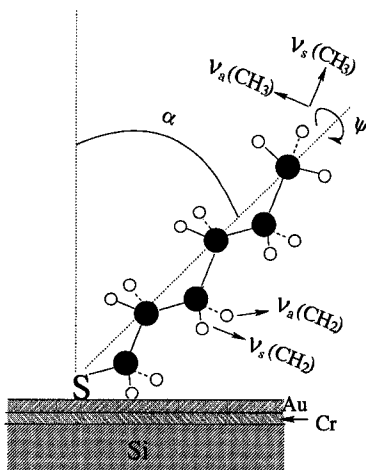
### 5.3 Mechanical Stability of SAMs on Au/Ti/Si substrate

#### 5.3.1 SAMs on evaporated Au/Ti/Si surface

Figure 5.6a shows the structure of SAMs formed on evaporated Au/Ti/Si surface. The peak position of  $\nu_a(\text{CH}_2)$  and  $\nu_s(\text{CH}_2)$  are exactly on 2918 and 2850  $\text{cm}^{-1}$ , indicating that this structure is very crystalline. After sonicating for 7 hours, the intensities of  $\nu_a(\text{CH}_2)$  and  $\nu_s(\text{CH}_2)$  increases slightly (Figure 5.6b), suggesting that some molecules have been peeled off by the cavitation force. However, the spectrum change is negligible. Thus, SAMs on evaporated Au/Ti/Si substrate are relatively more stable under this sonication power level.



(a) before sonication



(b) after sonication

Figure 5.5: Schematic illustration of an alkanethiolate adsorbed onto piranha-etched Au/Cr/Si surface before and after sonication. The arrows indicate the transition dipole moments for the following stretching modes:  $\nu_a(\text{CH}_3)$ ,  $\nu_s(\text{CH}_3)$ ,  $\nu_a(\text{CH}_2)$ ,  $\nu_s(\text{CH}_2)$ . The intensities of the infrared bands for these transition dipole moments depend on their projection along the surface normal.



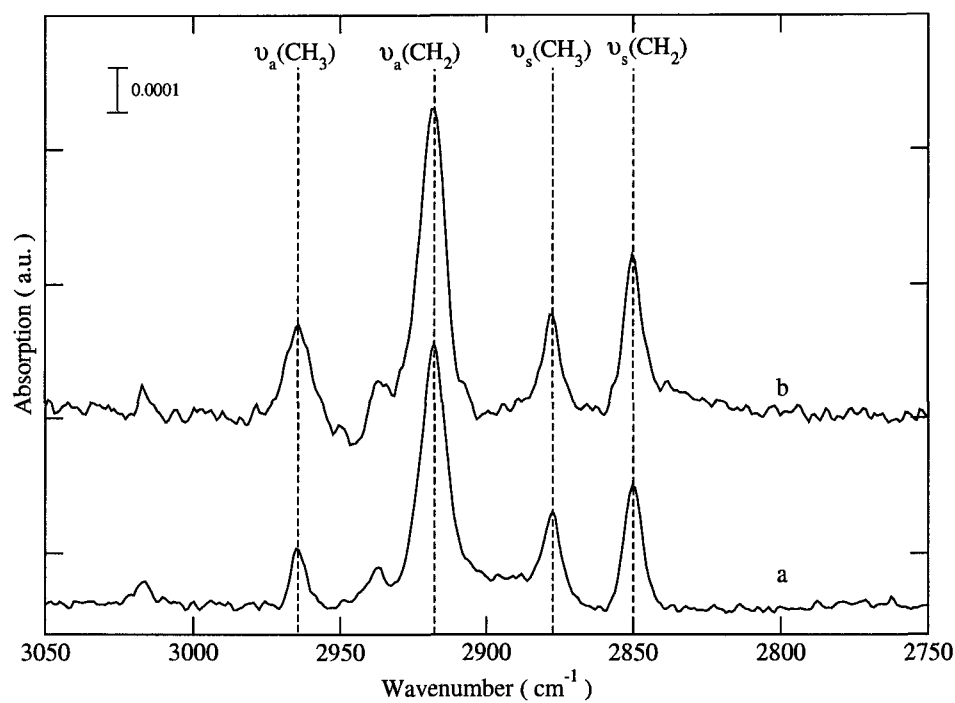


Figure 5.6: FTIR spectra of SAMs formed on evaporated Au/Ti/Si surface (a) before sonication; (b) after sonicating for 7 hours.

### 5.3.2 SAMs on chemically-etched Au/Ti/Si surface

Although the piranha-etched surface is microscopically smooth and SAMs are densely-packed in a small domain, the surfaces are macroscopically rough. As a consequence, the van der Waals force among molecules are relatively weak. In addition, the bond strength between molecule and substrate is reduced as piranha is known to leave a surface oxide on Au surface [22, 23]. Because of the above reasons, SAMs on piranha-etched Au/Ti/Si substrate are not very stable. Figure 5.7 shows the structural change under sonication for SAMs formed on the piranha-etched Au/Ti/Si surface. After sonicating for 7 hours, the methyl group intensities decrease and the methylene intensities increase. The  $\nu_a(\text{CH}_2)$  and  $\nu_s(\text{CH}_3)$  peaks broaden and result in a much broader band between the peaks. These information indicate that SAMs formed on piranha-etched Au/Ti/Si substrate are not stable.

### 5.3.3 SAMs on annealed Au/Ti/Si

SAMs formed on annealed Au/Ti/Si surfaces have been found to be very crystalline and densely-packed (Figure 4.2).

Annealing the Au substrate removes most organic contaminants and shaves the “rolling hills” on the evaporated Au surface. The high temperature during annealing leads to the fusion of small domains into larger ones. The strong S-Au bond and additional lateral interaction among molecules in the monolayer lead to sufficient stability under sonication. The associated spectra change is shown in Figure 5.8.

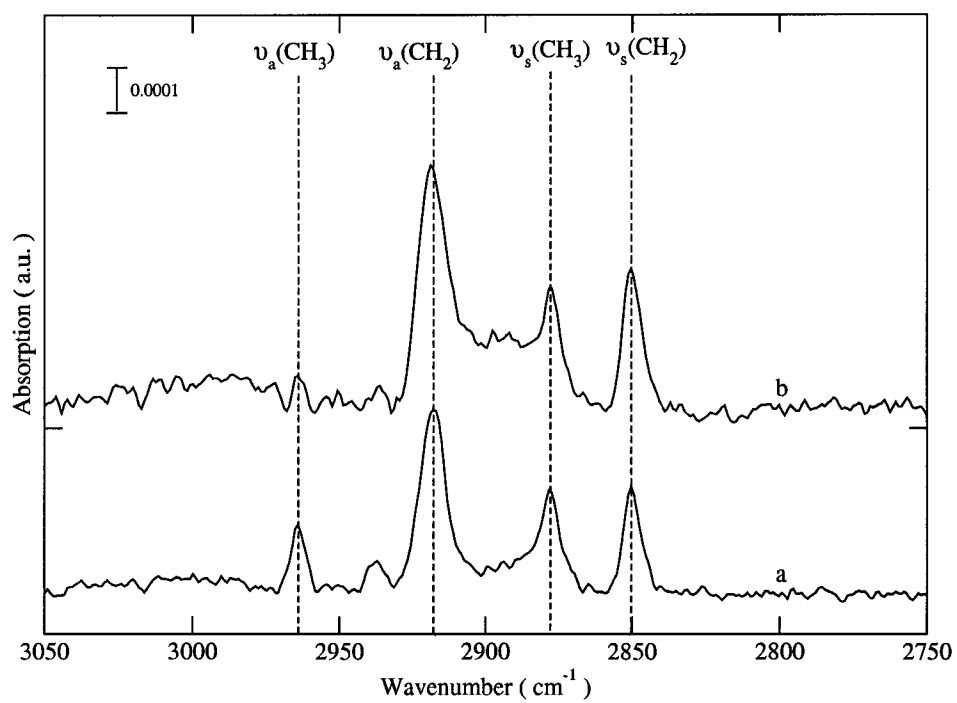


Figure 5.7: FTIR spectra of SAMs formed on chemically etched Au/Ti/Si surface (a) before sonication, (b) after sonicating for 7 hours

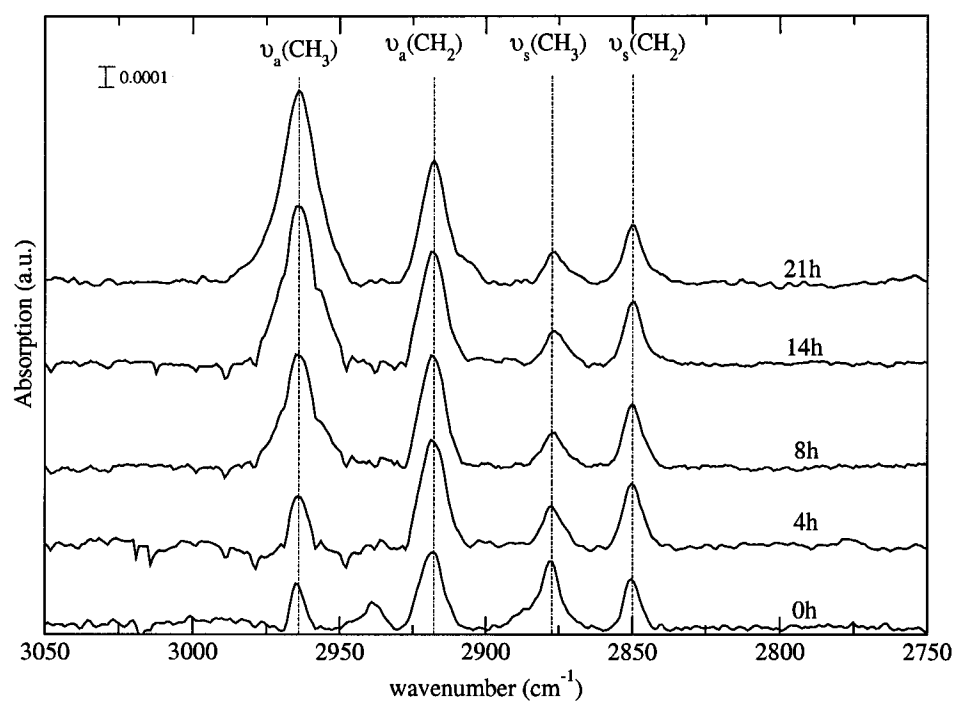
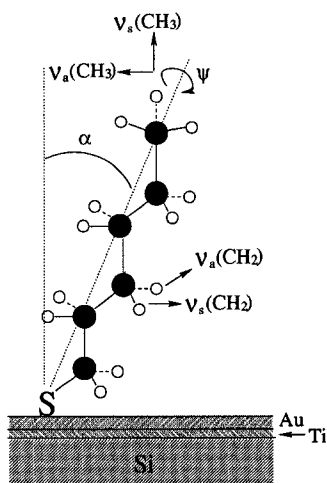


Figure 5.8: FTIR spectra of SAMs formed on annealed Au/Ti/Si surface subjected to ultrasonic vibration at various duration.

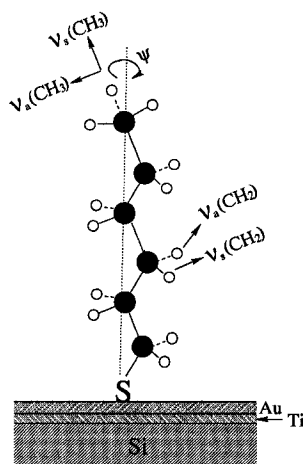
In FTIR spectra, the intensities of the infrared bands for  $\nu_a(\text{CH}_2)$ ,  $\nu_s(\text{CH}_2)$ ,  $\nu_a(\text{CH}_3)$  and  $\nu_s(\text{CH}_3)$  transition dipole moments depend on their projection along the surface normal direction [75]:

$$I^{SAM} \propto I^{bulk} \cos^2 \alpha \quad (5.1)$$

where  $I^{SAM}$  denotes the respective IR band intensity (absorbance) in the SAM spectrum;  $I^{bulk}$  denotes the corresponding band intensity in the bulk spectrum;  $\alpha$  is the angle between the specific dipole moment and the surface normal. Before sonication, the  $\nu_a(\text{CH}_3)$  is nearly perpendicular to the surface normal, and  $\cos \alpha$  is nearly zero. Thus, projection of  $\nu_a(\text{CH}_3)$  bond on the surface normal,  $I^{SAM}$ , is very small, resulting in a lower intensity in FTIR spectra (Figure 5.8). During sonication, the asymmetric methyl intensity  $\nu_a(\text{CH}_3)$  at  $2963 \text{ cm}^{-1}$  increases and the symmetric methyl intensity  $\nu_s(\text{CH}_3)$  at  $2879 \text{ cm}^{-1}$  decreases. The intensities of  $\nu_a(\text{CH}_2)$  and  $\nu_s(\text{CH}_2)$  remain the same (Figure 5.8), suggesting that the backbone chains are oriented more toward the surface normal. These features in the spectra provide evidence that SAM of  $\text{CH}_3(\text{CH}_2)_{17}\text{SH}$  on the annealed Au/Ti/Si has a structural change during sonication. The SAMs' structural change under sonication also are confirmed by its thickness measurements. Under sonication, the thickness of SAMs on annealed Au/Ti/Si substrate increases gradually (Figure 5.10), which is consistent with the FTIR result. The SAMs' structure on annealed Au/Ti/Si surface before and after sonication are schematically shown in Figure 5.9 [2, 3].



(a) Before sonication



(b) After sonication

Figure 5.9: Schematic illustration of an alkanethiolate adsorbed onto annealed Au/Ti/Si surface before (a) and after (b) sonication. The arrows indicate the transition dipole moments for the following stretching modes:  $\nu_a(\text{CH}_3)$ ,  $\nu_s(\text{CH}_3)$ ,  $\nu_a(\text{CH}_2)$ ,  $\nu_s(\text{CH}_2)$ . The intensities of the infrared bands for these transition dipole moments depend on their projection along the surface normal.

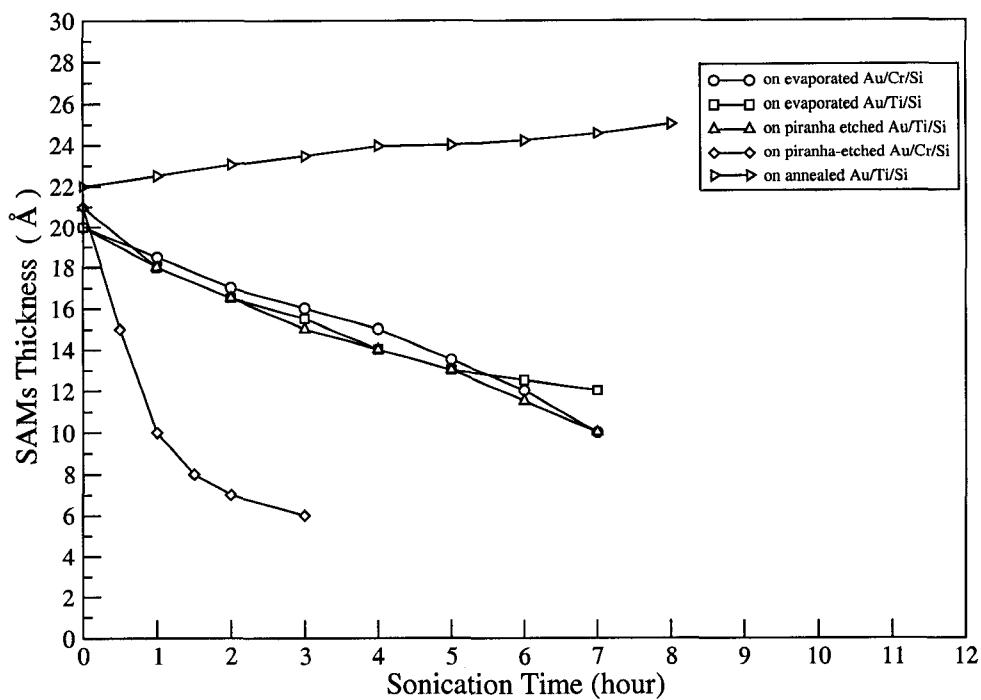


Figure 5.10: SAMs' thickness variation under sonication

#### 5.4 Ellipsometric Measurements

Following the thickness measurement procedures in Chapter 4, we characterized all SAMs' structural change under sonication by ellipsometric measurements.

Figure 5.10 shows the variation of SAMs' thickness under sonication. For SAMs formed on piranha-etched Au/Cr/Si surface, the thickness decreases

dramatically under sonication. This is consistent with the spectra results in Figure 5.4. In contrast, for SAMs formed on the annealed Au/Ti/Si surface, the thickness increases gradually. We have also measured the change in thickness of SAMs formed on evaporated Au/Cr/Si and Au/Ti/Si substrate, as well as those on piranha-etched Au/Ti/Si substrate. Under sonication, the thickness of the above SAMs all decrease gradually.

At the beginning of sonication, the exact thickness can be obtained by our spectroscopic ellipsometry measurements. The regressed  $\tan \Psi$  and  $\cos \Delta$  curves are both in near-perfect agreement with the measured  $\tan \Psi$  and  $\cos \Delta$  curves. After a certain time of sonication, neither of the above two curves matches well, especially the  $\tan \Psi$  curve. The fit, while subjected to significant possible sources of error, shows a structure that is qualitatively different from the original SAM. As the sonication time increases, the density and optical constant for SAMs consequently change. Thus, one could not regress to exact SAMs' thickness via Equation 4.1.



## CHAPTER 6

### DISCUSSION

In the literature, most self-assembled monolayers are formed on Au-coated Si substrates. The surface preparations are conducted within an ultrahigh vacuum chamber (less than  $10^{-6}$  torr), evaporated and deposited 100 to 200 nm Au onto the Si substrate. Because of the level of adhesion between the deposited Au film and the Si substrate is weak, an adhesion promotion layer, Cr or Ti, has always been used to enhance Au adhesion on Si substrates. However, no one has systematically studied the relationship between sub-layer, pretreatment, SAM's structure, and its properties. The results reported in Chapters 4 and 5 support a general understanding of the structure and stability of the alkanethiolate monolayers on Au/Cr/Si and Au/Ti/Si substrates.

#### **6.1 SAMs on Au/Cr/Ti substrates**

Following identical procedures, SAMs formed on annealed Au/Cr/Si and Au/Ti/Si substrates have totally different structures. SAMs on annealed Au/Ti/Si substrates are very crystalline and densely-packed (Figure 4.2)

while SAMs on annealed Au/Cr/Si substrate are in a chaotic state (Figure 4.1). After annealing the Au/Cr/Si substrate, white spots on the Au surface can be seen even by naked eyes as the chromium has diffused to the Au surface via grain boundaries and formed  $\text{Cr}_2\text{O}_3$ . The Cr diffusion effect is also confirmed in the literature [18, 76, 77]. With increased annealing time and temperature, there is an increase in surface chromium concentration and a corresponding decrease in surface Au concentration. The diffusion changes the composition and structure of the Au film, which have been confirmed by scanning tunneling microscopy (STM) and X-ray photoelectron spectroscopy measurements [76, 77]. These phenomena have caused significant concern regarding the long-term effects of chromium migration on film performance and durability and has motivated numerous studies on diffusion processes and their effects on film properties and performance [76, 77]. Zhao et al. [78] investigated the influence of Au thickness on the density of defects on SAMs. They found that the density of defects on SAMs increases as the thickness of Au decreases. A possible reason for this phenomenon is that Cr diffuses through the Au and acts as nucleation sites for defects; thinner Au films have a higher percentage of Cr than thicker films, resulting in a higher density of defects in thinner films than thicker ones (since Cr diffuses a shorter distance to reach the surface in the thinner Au films). Fan et al. have investigated the adhesion behavior of diamond on pure Cr and Ti substrates. Under indentation, they found diamond adheres better to Ti than it does to Cr [79]. This can be another reason that SAMs formed on Au/Cr/Si substrates are

less stable than those formed on the Au/Ti/Si substrates under sonication. For SAMs formed on Au/Cr/Si substrates, Cr can migrate to the Au surface slowly and reduce the strength of the S-Au bonds, which will affect SAMs long-term stability. Thus, Au/Ti/Si is the preferred substrate to form SAMs.

## 6.2 SAMs on Au/Ti/Si substrates

SAMs formed on Au/Ti/Si substrates are relatively more stable because Ti diffuses through Au more slowly than chromium. However, SAMs stability under sonication also depend on the surface pretreatment procedures.

Au prepared by evaporation at room temperature is typically polycrystalline and has a predominately (111) structure. The surface has a “rolling hills” topology and consists of crystallites of  $40 \text{ nm} \times 80 \text{ nm}$  and typical peak-to-valley heights of 3 nm between grains [18, 80]. Since organic contaminants from the ambient are easily adsorbed onto high energy Au surface, cleaning and etching steps are often part of the SAMs’ formation procedures. Piranha is often the choice for cleaning. SAMs formed on piranha-etched Au/Ti/Si substrates are more crystalline and densely-packed than SAMs formed on evaporated Au/Ti/Si substrates (Figure 4.2). However, piranha etches the Au surface and leaves a surface oxide which can affect the properties of the SAMs deleteriously [22, 23]. SAMs formed on piranha-etched Au/Ti/Si substrates have a poor stability than on evaporated Au/Ti/Si substrates (Figures 5.6 and 5.7).

Following the procedures in Chapter 3, heating the Au/Ti/Si substrates in

a gas flame results in a hydrophilic surface, indicating that all organics have been removed. The high temperature during annealing also causes the fusion of small domains into larger ones ( $\sim 200$  nm). Figure 3.2 shows the Au surface structure before and after annealing, which is confirmed by our AFM results. SAMs formed on annealed Au/Ti/Si substrates have a better structure than those on evaporated and piranha-etched Au/Ti/Si substrates (Figure 4.2). The intensities of the methylene peaks are largest for SAMs on freshly evaporated Au, least intense on annealed Au, and intermediate on piranha-etched Au. The differences in  $\nu_a(\text{CH}_2)$  intensity reflect different tilt angles for the polymethylene chains on these surfaces. The tilt of the hydrocarbon chain in SAMs is a result of the packing arrangement of the adsorbates on the Au surface [16]. The film thickness results, as determined by ellipsometry, also suggest that densely-packed SAMs are thicker, which is consistent with the interpretation of the FTIR spectrum.

SAMs formed on annealed Au/Ti/Si substrates have stronger Au-S bonds, additional lateral interactions among molecules and a densely-packed arrangement (Figure 4.2). These features result in sufficient stability under sonication (Figure 5.8).

### 6.3 Simulation

Apart from extensive experimental work [55, 56, 81], computer simulation provides a complementary method to elucidate the structure-property relationships of SAMs [82–84]. Simulating the response of SAMs to external

loads can provide valuable hints to their performance in service [57, 58]. SAMs under compressive load show a load-rate-dependent hysteresis in the compressive strain recovery, indicating that the mechanical properties of the SAM are best described by an anelastic model [55–58]. The above results also show that the compressive stress performed on SAMs is roughly proportional to the strain (the decreased thickness versus the original SAM thickness). Deducing a conclusion from the above simulation results, we anticipate that SAMs' thickness should increase under tensile stress.

Based on a simple model, Ulman et al. [84] provided a description of the relation between monolayer energy and the tilt angle  $\alpha$ . At ambient equilibrium state, the tilt angle is around  $30^\circ$ . As the energy (temperature) increases, the tilt angle decreases, and the thickness of the monolayer will increase [82, 83, 85, 86]. During sonication, SAMs on the substrates absorb the impact energy [87]. As the sonication time increases, the energy inside the SAMs increases, resulting in that the tilt angle of SAMs decreases.

In Chapter 5, we sonicated SAMs formed on various substrates, but only SAMs formed on annealed Au/Ti/Si substrates, as simulation predicts, increase the thickness and reduce the tilt angle. This implies that only SAMs on annealed Au/Ti/Si substrates have the ideal structure and stability.

Theoretically, the thickness of  $\text{CH}_3(\text{CH}_2)_{17}\text{SH}$  SAM formed on evaporated Au is  $22 \pm 1 \text{ \AA}$  [16]. Assuming that  $\text{CH}_3(\text{CH}_2)_{17}\text{SH}$  SAM is comprised of molecules with all-trans alkyl chains and with the chain axes normal to the substrate surface at the final stage of sonication (Figure 5.9b), the simulated

maximum thickness is 25 Å (where all portions are considered to be rigid rods and the molecule orientations have been restricted to being in the plane of the page) [88].

## CHAPTER 7

### CONCLUSIONS AND FUTURE WORK

#### 7.1 Conclusions

Applications of alkanethiol Self-Assembled Monolayers in many areas greatly depend on their structure and stability under various physical conditions. In the literature, SAMs are typically formed on Au/Cr/Si or Au/Ti/Si substrates. However, no one has systematically studied their difference. In this thesis, we have compared the structure and stability of SAMs formed on Au/Ti/Si and Au/Cr/Si substrates using different pretreatment procedures. The results are listed below:

1. Titanium is the preferred material as it diffuses through Au more slowly than chromium. In order to increase SAMs' long-term stability, thinner interlayer ( $\sim 50$  Å Cr [13] or Ti [20]) and thicker Au layer (1500  $\sim$  2000 Å) should be used.
2. Although SAMs formed on piranha-etched Au substrates have a more densely-packed structure than on evaporated Au (Figures 4.1 and 4.2), piranha-etching is not a good method to use for cleaning of substrate.

Piranha etches Au surface and leaves a surface oxide which can affect the properties of SAMs deleteriously.

3. Annealing the Au substrate not only removes all organic contaminants, it also shaves the “rolling hills” on evaporated Au surface and provides an ideally smooth Au surface. SAMs formed on annealed Au/Ti/Si surfaces are densely-packed and have the best stability.
4. The stability of SAMs depends on the force between Au-S bond and the van der Waals force between the thiol and its surrounding molecules. Stable SAMs can only be formed on smooth surfaces with completed wetting. The results define the relationship between substrate preparation, SAMs’ structure and properties.

## 7.2 Future Work

Annealing Au/Ti/Si and Au/Cr/Si substrates above 5 min will cause Cr and Ti to migrate to the Au surface, reducing the Au-S affinity and decreasing SAMs’ stability. An increasingly popular substrate in self-assembled monolayers studies is an epitaxial Au layer supported on mica. Mica has a layered structure, and the act of simply peeling apart the mica sheets can produce atomically flat large surface areas. The crystallinity and morphology of the Au films that form on the mica are dependent on the temperature of the mica during the deposition [89, 90]. Au evaporated onto mica held at high temperature between 250 – 450°C contains Au(111) layer that consists of



flat terraces of about  $0.2 \mu\text{m}$  in diameter [18, 90–93]. Another advantage for Au evaporated on high temperature mica substrate is that there is no need to have a promotion layer and no sublayer diffusion problem, while Au supported on Si requires Ti or Cr as an adhesion sublayer. The procedures detailed in this thesis could be repeated for this substrate. We expect that SAMs formed on Au coated mica substrate should have a more crystalline structure and better stability.

## BIBLIOGRAPHY

- [1] E. Delamarche, B. Michel, H. Kang, and Ch. Gerber. Thermal stability of self-assembled monolayers. *Langmuir*, 10:4103, 1994.
- [2] P. E. Laibinis, G. M. Whitesides, A. N. Parikh, Y. T. Tao, D. L. Allara, and R. G. Nuzzo. Comparison of the structures and wetting properties of self-assembled monolayers of *n*-alkanethiols on the coinage metal-surfaces, Cu, Ag, Au. *J. Am. Chem. Soc.*, 113(19):7152, 1991.
- [3] D. L. Allara. Spontaneously organized molecular assemblies. 2. quantitative infrared spectroscopic determination of equilibrium structures of solution-adsorbed *n*-alkanoic acids on an oxidized aluminum surface. *Langmuir*, 1:52–66, 1985.
- [4] C. D. Bain and G. M. Whitesides. Modeling organic-surfaces with self-assembled monolayers. *Angew. Chem. Int. Ed.*, 28(4):506, 1989.
- [5] G. M. Whitesides and P. E. Laibinis. Wet chemical approaches to the characterization of organic-surfaces-self-assembled monolayers, wetting, and the physical organic-chemistry of the solid liquid interface. *Langmuir*, 6:87, 1990.

- [6] A. Ulman. *An introduction to ultrathin organic films from Langmuir-Blodgett to Self-Assembly*. Academic Press: Boston, 1991.
- [7] L. H. Dubois and R. G. Nuzzo. Synthesis, structure, and properties of model organic-surfaces. *Ann. Rev. Mater. Sci.*, 43:437, 1992.
- [8] Y. Xia and G. M. Whitesides. Soft lithography. *Angew. Chem. Int. Ed.*, 37:550, 1998.
- [9] W. C. Bigelow, D. L. Pickett, and W. A. Zisman. *J. Colloid Interface*, page 513, 1946.
- [10] R. L. Shuler and W. A. Zisman. Wave-damping and film-pressure studies of polydimethylsiloxane monolayers on organic liquid substrates. *J. Phys. Chem.*, pages 1397–1405, 1975.
- [11] M. K. Bernett and W. A. Zisman. Surface chemical properties of highly fluorinated polymers. *Adv. Chem. Ser.*, 8:199–211, 1975.
- [12] R. G. Nuzzo, F. A. Fusco, and D. L. Allara. Spontaneously organized molecular assemblies .3. preparation and properties of solution adsorbed monolayers of organic disulfides on gold surfaces. *J. Am. Chem. Soc.*, 109:2358, 1987.
- [13] C. D. Bain, E. B. Troughton, Y. T. Tao, J. Evall, G. M. Whitesides, and R. G. Nuzzo. Formation of monolayer films by spontaneous assembly of organic thiols from solution onto gold. *J. Am. Chem. Soc.*, 111:321, 1989.

- [14] W. Guo and G. K. Jennings. Use of underpotentially deposited metals on gold to affect the surface-catalyzed formation of polymethylene films. *Langmuir*, 2002.
- [15] A. Todd Lusk and G. Kane Jennings. Characterization of self-assembled monolayers formed from sodium *s*-alkyl thiosulfates on copper. *Langmuir*, 17(25):7830–7836, 2001.
- [16] G. K. Jennings and P. E. Laibinis. Self-assembled *n*-alkanethiolate monolayers on underpotentially deposited adlayers of silver and copper on gold. *J. Am. Chem. Soc.*, 119:5208–5214, 1997.
- [17] G. K. Jennings and P. E. Laibinis. Underpotentially deposited metal layers of silver provide enhanced stability to self-assembled alkanethiol monolayers on gold. *Langmuir*, 12:6173, 1996.
- [18] P. E. Laibinis, B. J. Palmer, S. W. Lee, and G. K. Jennings. The synthesis of organothiols and their assembly into monolayers on gold. *THIN FILMS*, 24, 1998.
- [19] R. G. Nuzzo, L. H. Dubois, and D. L. Allara. Fundamental-studies of microscopic wetting on organic-surfaces .1. formation and structural characterization of a self-consistent series of polyfunctional organic monolayers. *J. Am. Chem. Soc.*, 112(2):558, 1990.
- [20] V. J. Angelico, S. A. Mitchell, and V. H. Wysocki. Low-energy ion-

- surface reactions of pyrazine with two classes of self-assembled monolayers: Influence of alkyl chain orientation. *Anal. Chem.*, 72:2603, 2000.
- [21] F. Zamborini and Richard M. Crooks. Corrosion passivation of gold by *n*-alkanethiol self-assembled monolayer: Effect of chain length and end group. *Langmuir*, 14:3279, 1998.
- [22] H. Ron and I. Rubinstein. Alkanethiol monolayers on preoxidized gold. encapsulation of gold oxide under an organic monolayer. *Langmuir*, 10:4566, 1994.
- [23] H. Ron, S. Matlis, and I. Rubinstein. Self-assembled monolayers on oxidized metals. 2. gold surface oxidative pretreatment, monolayer properties, and depression formation. *Langmuir*, 14:1116, 1998.
- [24] Y. Golan, L. Margulis, S. Matlis, and I. Rubinstein. Vacuum-deposited gold-films .2. role of the crystallographic orientation of oxide-covered silicon substrates. *J. Electrochem. Soc.*, 142(5):1629, 1995.
- [25] D. H. Kim, J. Noh, M. Hara, and H. Lee. An adsorption process study on the self-assembled monolayer formation of octadecanethiol chemisorbed on gold surface. *Bull. Korean Chem. Soc.*, 22(3):276, 2001.
- [26] S. E. Creager, L. A. Hockett, and G. K. Rowe. Consequences of microscopic surface-roughness for molecular self-assembly. *Langmuir*, 8:854, 1992.

- [27] Lili Duan and Simon J. Garret. Self-assembled monolayers of 6-phenyl-n-hexanethiol and 6-(p-vinylphenyl)-n-hexanethilo on Au(111): An investigation of structure, stability, and reactivity. *Langmuir*, 17:2986–2994, 2001.
- [28] VWR scientific products. *Owner's manual for 75D aquasonic cleaner*. VWR scientific products, 2001.
- [29] V. Kaajakari, A. Sathaye, and A. Lal. *The 11th International Conference on Solid-State Sensors and Actuators, Munich Germany, June 10-14, 2001*.
- [30] Frank Schreiber. Structure and growth of self-assembling monolayers. *Progress in Surface Science*, 65:151–256, 2000.
- [31] I. Doudevski, W. A. Hayes, J. T. Woodward, and D. K. Schwartz. Atomic force microscope imaging of molecular aggregation during self-assembled monolayer growth. *Colloids and Surfaces A*, 174:233, 2000.
- [32] Y. S. Shon and T. R. Lee. Chelating self-assembled monolayers on gold generated from spiroalkanedithiols. *Langmuir*, 15:1136, 1999.
- [33] D. S. Karpovich and G. J. Blanchard. Direct measurement of the adsorption kinetics of alkanethiolate self-assembled monolayers on a microcrystalline gold surface. *Langmuir*, 10:3315, 1994.
- [34] S. Jiang. Molecular simulation studies of self-assembled monolayers of alkanethiols on au(111). *Molecular Physics*, 100(14):2261, 2002.

- [35] H. Gronbeck, A. Curioni, and W. Andreoni. Thiols and disulfides on the Au(111) surface: The headgroup-gold interaction. *J. Am. Chem. Soc.*, 122(16):3839, 2000.
- [36] H. Sellers, A. Ulman, Y. Shnidman, and J. E. Eilers. Structure and binding of alkanethiolates on gold and silver surfaces - implications for self-assembled monolayers. *J. Am. Chem. Soc.*, 115(21):9389, 1993.
- [37] R. G. Nuzzo and D. L. Allara. *J. Am. Chem. Soc.*, 105:4481, 1983.
- [38] R. G. Nuzzo, B. R. Zegarski, and L. H. Dubois. Fundamental-studies of the chemisorption of organosulfur compounds on Au(111) - implications for molecular self-assembly on gold surfaces. *J. Am. Chem. Soc.*, 109:773, 1987.
- [39] R. G. Nuzzo, R. G. Korenic, and L. H. Dubois. Studies of the temperature-dependent phase-behavior of long-chain normal-alkyl thiol monolayers on gold. *J. Chem. Phys.*, 93(1):767, 1990.
- [40] L. H. Dubois and R. G. Nuzzo. Synthesis, structure, and properties of model organic surfaces. *Annu. Rev. Phys. Chem.*, 43:437-463, 1992.
- [41] A. I. Kitaigorodskii. *Organic Chemistry Crystallography*. Consultants Bureau, New York, 1961.
- [42] N. Camillone, C. E. D. Chidsey, and G. J. Scoles. Superlattice structure at the surface of a monolayer of octadecanethiol self-assembled on Au(111). *J. Chem. Phys.*, 98:3505, 1993.

- [43] P. Fenter, P. Eisenberger, and K. Liang. Chain-length dependence of the structures and phases of  $\text{CH}_3(\text{CH}_2)_{n-1}\text{SH}$  self-assembled on Au(111). *Phys. Rev. Lett.*, 70(16):2447, 1993.
- [44] P. Fenter, A. Eberhardt, and P. Eisenberger. Self-assembly of n-alkyl thiols as disulfides on Au(111). *Science*, 266(5188):1216, 1994.
- [45] G. E. Poirier and M. J. Tarlov. The  $c(4 \times 2)$  superlattice of *n*-alkanethiol monolayers self-assembled on Au(111). *Langmuir*, 10:2853–2856, 1994.
- [46] C. D. Bain, H. A. Biebuyck, and G. M. Whitesides. Comparison of self-assembled monolayers on gold - coadsorption of thiols and disulfides. *Langmuir*, 5(3):723, 1989.
- [47] H. A. Biebuyck and G. M. Whitesides. Interchange between monolayers on gold formed from unsymmetrical disulfides and solutions of thiols - evidence for sulfur sulfur bond-cleavage by gold metal. *Langmuir*, 9(7):1766–1770, 1993.
- [48] H. A. Biebuyck, C. D. Bain, and G. M. Whitesides. Comparison of organic monolayers on polycrystalline gold spontaneously assembled from solutions containing dialkyl disulfides or alkenethiols. *Langmuir*, 10(6):1825, 1994.
- [49] M. M. Walczak, C. Chung, S. M. Stole, C. A. Widrig, and M. D. Porter. Structure and interfacial properties of spontaneously adsorbed normal-



- alkanethiolate monolayers on evaporated silver surfaces. *J. Am. Chem. Soc.*, 113(7):2370, 1991.
- [50] S. C. Chang, I. Chao, and Y. T. Tao. Structure of self-assembled monolayers of aromatic-derivatized thiols on evaporated gold and silver surfaces: Implication on packing mechanism. *J. Am. Chem. Soc.*, 116(15):6792, 1994.
- [51] Y. T. Tao, C. C. Wu, J. Y. Eu, and W. L. Lin. Structure evolution of aromatic-derivatized thiol monolayers on evaporated gold. *Langmuir*, 13(15):4018, 1997.
- [52] S. Y. Lin, T. K. Tsai, C. M. Lin, and C. H. Chen. Structures of self-assembled monolayers of n-alkanoic acids on gold surfaces modified by underpotential deposition of silver and copper: Odd-even effect. *Langmuir*, 18(14):5473, 2002.
- [53] B. Liedberg and J. M. Cooper. *Bioanalytical applications of self-assembled monolayers. Immobilized biomolecules in analysis: A practical approach*. Oxford University Press, 1998.
- [54] M. D. Porter, T. B. Bright, D. L. Allara, and C. E. D. Chidsey. Spontaneously organized molecular assemblies .4. structural characterization of normal-alkyl thiol monolayers on gold by optical ellipsometry, infrared-spectroscopy, and electrochemistry. *J. Am. Chem. Soc.*, 109:3559, 1987.

- [55] S. A. Joyce, R. C. Thomas, J. E. Houston, T. A. Michalske, and R. M. Crooks. Mechanical relaxation of organic monolayer films measured by force microscopy. *Phys. Rev. Lett.*, 68(18):2790, 1992.
- [56] R. C. Thomas, J. E. Houston, T. A. Michalske, and R. M. Crooks. The mechanical response of gold substrates passivated by self-assembled monolayer films. *Science*, 259:1883, 1993.
- [57] R. Henda, M. Grunze, and A. J. Pertsin. Static energy calculations of stress-strain behavior of self-assembled monolayers. *Tribology Letters*, 5:191, 1998.
- [58] R. Henda. Simulation of self-assembled monolayers under normal stress. *AIChE Journal*, 46(6):1275, 2000.
- [59] C. Schonenberger, J. Jorritsma, J. A. M. Sondag-Huethorst, and L. G. J. Fokkink. Domain structure of self-assembled alkanethiol monolayers on gold. *J. Phys. Chem.*, 99:3259, 1995.
- [60] T. Ishida, S. Yamamoto, W. Mizutani, M. Motomatsu, H. Tokumoto, H. Hokari, H. Azebara, and Masamichi. Evidence for cleavage of disulfides in the self-assembled monolayer on Au(111). *Langmuir*, 13:3261, 1997.
- [61] G. Kataby, T. Prozorov, Y. Koltypin, H. Cohen, C. N. Sukenik, A. Ulman, and A. Gedanken. Self-assembled monolayer coatings on amor-

- phous iron and iron oxide nanoparticles: thermal stability and chemical reactivity studies. *Langmuir*, 13:6151, 1997.
- [62] J. B. Schlenoff, M. Li, and H. Ly. Stability and self-exchange in alkanethiol monolayers. *J. Am. Chem. Soc.*, 117:6173, 1995.
- [63] J. Huang, D. A. Dahlgren, and J. C. Hemminger. Photopatterning of self-assembled alkanethiolate monolayers on gold: A simple monolayer photoresist utilizing aqueous chemistry. *Langmuir*, 10:626, 1994.
- [64] L. H. Dubois and B. R. Zegarski. Molecular ordering of organosulfur compounds on Au(111) and Au(100): adsorption from solution and in ultrahigh vacuum. *J. Chem. Phys.*, 98(1):678, 1993.
- [65] D. M. Jaffey and R.J. Madix. Reactivity of sulfur-containing molecules on noble metal surfaces. 2. *tert*-butyl thioalcohol on Au(110). *J. Am. Chem. Soc.*, 116:3012, 1994.
- [66] D. M. Jaffey and R. J. Madix. The reactivity of sulfur-containing molecules on noble metal surfaces III. ethanethiol on Au(110) and Ag(110). *surf. Sci.*, 311:159, 1994.
- [67] J. Li, K. Liang, N. Camillone, T. Leung, and G. Scoles. The structure of n-octadecane thiol monolayers self-assembled on Au(001) studied by synchrotron x-ray and helium atom diffraction. *J. Chem. Phys.*, 102(12):5012, 1995.

- [68] S. W. Tam-Chang, H. A. Biebuyck, G. M. Whitesides, N. Jeon, and R. G. Nuzzo. Self-assembled monolayers on gold generated from alkanethiols with the structure  $\text{RNHCOCH}_2\text{SH}$ . *Langmuir*, 11:4371, 1995.
- [69] J. Schneir, R. Sonnenfeld, O. Marti, P.K. Hansma, J.E. Demuth, and R.J. Hamers. Tunneling microscopy, lithography, and surface diffusion on an easily prepared, atomically flat gold surface. *J. Appl. Phys.*, 63:717, 1988.
- [70] J. Yang, J. Han, K. Isaacson, and D. Y. Kwok. Effects of surface defects, polycrystallinity, and nanostructure of self-assembled monolayers for octadecanethiol adsorbed onto au on wetting and its surface energetic interpretation. *Langmuir*, 19:9231, 2003.
- [71] A. R. Sandy, S.G. J. Mochrie, D. M. Zehner, K. G. Huang, and D. Gibbs. Structure and phases of Au(111) surface: X-ray-scattering measurements. *Phys. Rev. B*, 43:4667, 1991.
- [72] Anton Puskar. *The use of high-intensity ultrasonics*. Veda, Publishing House of the Slovak Academy of Sciences, 1982.
- [73] R. G. Nuzzo. Fundamental studies of microscopic wetting on organic surfaces. 1. formation and structural characterization of a self-consistent series of polyfunctional organic monolayers. *J. Am. Chem. Soc.*, 112(2):558–569, 1990.

- [74] F. P. Zamborini and R. M. Crooks. Corrosion passivation of gold by *n*-alkanethiol self-assembled monolayers: Effect of chain length and end group. *Langmuir*, 14:3279–3286, 1998.
- [75] R. Arnold, A. Terfort, and C. Woll. Determination of molecular orientation in self-assembled monolayers using ir absorption intensities: The importance of grinding effects. *Langmuir*, 17(16):4980, 2001.
- [76] N.R. Moody, D.P. Adams, D. Medlin, T. Headley, N. Yang, and A. Volinsky. Effect of diffusion on interfacial fracture of gold-chromium hybrid microcircuit films. *International Journal of Fracture*, 2003.
- [77] M. A. George, W. S. Glaunsinger, T. Thundat, and S. M. Lindsay. Electrical, spectroscopic, and morphological investigation of chromium diffusion through gold films. *Thin Solid Films*, 1990.
- [78] X. Zhao, J. L. Wilbur, and G. M. Whitesides. Using two-stage chemical amplification to determine the density of defects in self-assembled monolayers of alkanethiolates on gold. *Langmuir*, 12(13):3257, 1996.
- [79] Q.H. Fan, J. Gracio, E. Pereira, N. Ali, and W. Ahmed. Study of diamond adhesion behavior on chromium and titanium for obtaining adherent diamond coatings on steel. *Journal of materials research*, 2000.
- [80] J. P. Folkers, P. E. Laibinis, and G. M. Whitesides. Self-assembled monolayers of alkanethiols on gold - comparisons of monolayers contain-

- ing mixtures of short-chain and long-chain constituents with  $\text{CH}_3$  and  $\text{CH}_2\text{OH}$  terminal groups. *Langmuir*, 8(5):1330–1341, 1992.
- [81] G. Y. Liu and M. B. Salmeron. Reversible displacement of chemisorbed *n*-alkanethiol molecules on Au(100) surface: an atomic force microscopy study. *Langmuir*, 10:367, 1994.
- [82] J. Hautman and M. L. Klein. Molecular dynamics simulation of the effects of temperature on a dense monolayer of long-chain molecules. *J. Chem. Phys.*, 93:7483, 1990.
- [83] L. Zhang, W. A. Goddard III, and S. Jiang. Molecular simulation study of the  $c(4 \times 2)$  superlattice structure of alkanethiol self-assembled monolayers on Au(111). *J. Chem. Phys.*, 117(15):7342, 2002.
- [84] A. Ulman, J. E. Eilers, and N. Tillman. Packing and molecular-orientation of alkanethiol monolayers on gold surfaces. *Langmuir*, 5:1147, 1989.
- [85] A. V. Shevade, J. Zhou, M. T. Zin, and S. Jiang. Phase behavior of mixed self-assembled monolayers of alkanethiols on Au(111): A configurational-bias monte carlo simulation study. *Langmuir*, 17(24):7566, 2001.
- [86] Wen Mar and M. L. Klein. Molecular-dynamics study of the self-assembled monolayer composed of  $\text{S}(\text{CH}_2)_{14}\text{CH}_3$  molecules using an all-atoms model. *Langmuir*, 10(1):188, 1994.

- [87] B. Bhushan. *Principles and Applications of Tribology*. Wiley, New York, 1999.
- [88] S. D. Evans, E. Urankar, A. Ulman, and N. Ferris. Self-assembled monolayers of alkanethiols containing a polar aromatic group - effects of the dipole position on molecular packing, orientation, and surface wetting properties. *J. Am. Chem. Soc.*, 113(11):4121, 1991.
- [89] C. E. D. Chidsey, D. N. Loiacono, T. Sleator, and S. Nakahara. Stm study of the surface-morphology of gold on mica. *Surface Science*, 200(1):45–66, 1988.
- [90] M. C. Barnes, D-Y. Kim, and N. M. Hwang. The mechanism of gold deposition by thermal evaporation. *Journal fo Ceramic Processing Research*, 2000.
- [91] M. Levin, A. Laakso, H.E.M. Niemi, and P. Hautojarvi. Evaporation of gold thin films on mica: effect of evaporation parameters. *Applied Surface Science*, 1997.
- [92] Z.H. Lui and N.M.D. Norman. Studies using afm and stm of the correlated effects of the deposition parameters on the topography of gold on mica. *Thin Solid Films*, 1997.
- [93] L.H. Guo, J.S. Facci, G. McLendon, and R. Mosher. Effect of gold topography and surface pretreatment on the self-assembly of alkanethiol monolayers. *Langmuir*, 10:4588–4593, 1994.